Aalto University

OPEN ACCESS

This is an electronic reprint of the original article.
This reprint may differ from the original in pagination and typographic detail.

Salpakari, Jyri; Rasku, Topi; Lindgren, Juuso; Lund, Peter D.

Flexibility of electric vehicles and space heating in net zero energy houses

Published in:
Applied Energy

DOI:
10.1016/j.apenergy.2017.01.005

Published: 15/03/2017

Document Version
Peer-reviewed accepted author manuscript, also known as Final accepted manuscript or Post-print

Published under the following license:
CC BY-NC-ND

Please cite the original version:
Salpakari, J., Rasku, T., Lindgren, J., & Lund, P. D. (2017). Flexibility of electric vehicles and space heating in net zero energy houses: an optimal control model with thermal dynamics and battery degradation. *Applied Energy*, *190*, 800-812. https://doi.org/10.1016/j.apenergy.2017.01.005

This material is protected by copyright and other intellectual property rights, and duplication or sale of all or part of any of the repository collections is not permitted, except that material may be duplicated by you for your research use or educational purposes in electronic or print form. You must obtain permission for any other use. Electronic or print copies may not be offered, whether for sale or otherwise to anyone who is not an authorised user.

Flexibility of electric vehicles and space heating in net zero energy houses: an optimal control model with thermal dynamics and battery degradation

Jyri Salpakari[a,*], Topi Rasku[a], Juuso Lindgren[a], Peter D. Lund[a]

[a] *New Energy Technologies Group, Department of Applied Physics, School of Science, Aalto University, P.O.Box 15100, FI-00076 AALTO (Espoo), Finland*

Abstract

With the increasing penetration of distributed renewable energy generation and dynamic electricity pricing schemes, applications for residential demand side management are becoming more appealing. In this work, we present an optimal control model for studying the economic and grid interaction benefits of smart charging of electric vehicles (EV), vehicle-to-grid, and space heating load control for residential houses with on-site photovoltaics (PV). A case study is conducted on 1–10 net zero energy houses with detailed empirical data, resulting in 8–33% yearly electricity cost savings per household with various electric vehicle and space heating system combinations. The self-consumption of PV is also significantly increased.

Additional benefits through increasing the number of cooperating households are minor and saturate already at around 3–5 households. Permitting electricity transfer between the houses and EV charging stations at workplaces increases self-sufficiency significantly, but it provides limited economic benefit. The additional cost savings from vehicle-to-grid compared to smart charging are minor due to increased battery degradation, despite a significant self-sufficiency increase. If the optimization is conducted without taking the battery degradation cost into account, the added monetary value of vehicle-to-grid can even be negative due to the unmanaged degradation. Neglecting battery degradation completely leads to overestimation of the vehicle-to-grid cost benefit.

Keywords: Energy management, net zero energy, photovoltaics, electric vehicles, space heating load control, linear programming

*Corresponding author. Tel.: +358 50 433 1262, e-mail: jyri.salpakari@aalto.fi

Nomenclature

Abbreviations

A/C	air conditioning
BEV	battery electric vehicle
CHP	combined heat and power
COP	coefficient of performance
DHW	domestic hot water
DOD	depth of discharge
DSM	demand side management
E10	ethanol-fuel mixture with 10% ethanol
GSHP	ground-source heat pump
HVAC	heating, ventilation, and air conditioning
ICE	internal combustion engine
LMO	lithium manganese oxide
LP	linear programming
MG	microgrid
MILP	mixed-integer linear programming
net-ZEB	net zero energy
NMC	nickel manganese cobalt
PDF	probability density function
PEV	plug-in electric vehicle
PHEV	plug-in hybrid electric vehicle
PV	photovoltaic
RE	renewable energy
SC	smart charging
SEA	Swedish Energy Agency
SHLC	space heating load control
SOC	state of charge of battery
TRNSYS	Transient System Simulation Tool
V2G	vehicle-to-grid
VRE	variable renewable energy

Symbols

A	surface area, heat transfer and capacity matrix
a_c	capacity severity factor in battery ageing model
B	heat transfer and capacity matrix
b	battery ageing model fitting parameter
C	heat capacity
c	specific heat capacity, battery ageing model fitting parameter
D	power draw required by EV driving
E	energy
F	fuel energy
f	probability density function
G	grid or market interaction power
g	vehicle grid-connection indicator
H	heat transfer coefficient
h	height
i	general integer index
J	ampere-hour throughput
j	general integer index
k	general integer index
L	battery capacity loss ratio
N	number
P	electric power
p	price, cost
Q	ampere-hour capacity of battery
R_g	universal gas constant
r	driving mode parameter in PEV battery ageing model
S	electric power for vehicle charging or discharging in home grid
SOC	state-of-charge
T	temperature
t	time
U	voltage, U-value
V	volume
w	indicator of vehicle location at workplace charging station
y	electricity transmission to workplace indicator
z	battery ageing model fitting parameter

α	coefficient of performance
α_c	battery ageing model fitting parameter
$\boldsymbol{\beta}$	matrix in analytic solution of differential equation
β_c	battery ageing model fitting parameter
$\boldsymbol{\gamma}$	matrix in analytic solution of differential equation
γ_c	battery ageing model fitting parameter
$\boldsymbol{\epsilon}$	matrix in analytic solution of differential equation
$\boldsymbol{\zeta}$	matrix in analytic solution of differential equation
η	efficiency
κ	supply water temperature coefficient of the heating system
Λ	effective surface area of vehicle cabin
μ	air exchange rate
ν	battery self-discharge rate
τ	supply water temperature constant of the heating system
$\bar{\upsilon}$	total heat transfer factor to interior from radiant floor
Φ	total thermal power
ϕ	thermal power
φ	passive heat gain
Ψ	total electric power in electric heating or cooling
ψ	electric power in electric heating or cooling

Subscripts and superscripts

0	reference value
$+$	charging, heating
$-$	consumption, cooling, discharging
ac	activation
app	appliance
b	battery, buy
c	cabin
$cell$	cell
Ca	Carnot
d	degradation
do	door
dhw	domestic hot water
e	exterior (ambient air)
F	fuel
f	fee, floor
fl	floor
g	ground, going to work
$HVAC$	heating, ventilation and air conditioning
h	house
i	interior
in	inlet
m	market
max	maximum
min	minimum
ppl	people
r	retail, returning from work
ro	roof
s	sell
sol	solar
sup	supply
$system$	system
ref	reference value
v	vehicle
w	work
wa	wall
wi	window

1. Introduction

Concerns about climate change drive the use of variable renewable energy (VRE) in electricity production, most notably solar and wind generation [1]. Without additional flexibility, large scale VRE generation cannot be fully utilized without compromising power system reliability and safety [1].

Demand side management (DSM) can compensate for lack of flexibility by establishing control of the consumption. Ideal DSM appliances have a lot of idle time and are shiftable, i.e. the exact timing of their power draw is irrelevant to the end user. Therefore, space heating and heating domestic hot water (DHW) with heat pumps and thermal energy storage (TES), and charging plug-in electric vehicles (PEVs) are promising candidates for DSM applications [2]. Moreover, they fit with electrification of transport and heating sectors, and energy efficiency of buildings, which are seen as key pathways to low-carbon energy systems along with increase in VRE use [3]. Heat pumps are a well-established technology rapidly growing its market share, with a total thermal capacity of 66.3 GW in Europe in 2014 and 10% annual growth [4, 5]. The required thermal energy storage can come from building mass or separate thermal storage devices, both of which are well-established technologies [6]. Plug-in electric vehicles are marginal at the moment, with 180 000 vehicles or 0.02% of total passenger car stock worldwide in 2012, but they are expected to grow their market share to over 20 million vehicles by 2050 [7].

Since PEVs represent a significant extra load for the utility grid [8], smart charging (SC) will be a crucial part of vehicle electrification in order to avoid adverse effects of uncoordinated charging on the utility grid, e.g. power losses and voltage deviations [9, 10, 8]. In addition to avoiding overloading the power grid, SC can provide benefits such as cost savings [11], peak load reduction [12], and increased battery lifetime by avoiding high SOC (state of charge) values [13]. As most privately owned vehicles spend significant amounts of time parked [14, 8], a controlled fleet of grid-connected PEVs could provide a significant contribution to the flexibility of power systems for e.g. ancillary services or balancing VRE sources [15, 8]. Balancing VRE production with PEVs would also increase the renewable energy share of PEV energy consumption, required for the full environmental benefits of PEVs [7]. Vehicle-to-grid (V2G) augments SC by feeding electricity from the PEVs back to the grid, making the PEVs distributed short-term electricity storages with high potential as a buffer for VRE generation or as a peak power resource [16]. However, the additional cycling due to V2G decreases the battery lifetime [8].

This work presents a model for quantifying the economic and grid interaction benefits achievable with SC, V2G and space heating load control (SHLC) for residential prosumers with photovoltaic (PV) generation. More specifically, a linear programming (LP) model of a 1–10 household residential microgrid (MG) with PEVs and PV generation is constructed, and cost-optimal control of the PEV and space heating and cooling loads is solved. Space heating and cooling are provided energy-efficiently with ground-source heat pumps (GSHP) and ground source free cooling. Battery degradation is included in the model.

A case study on energy-efficient net zero energy buildings (net-ZEB) set in Norrköping, Sweden is conducted with several combinations and dimensionings of the technologies, using detailed empirical data.

The overall topic of optimal operation of flexible energy systems with VRE has been widely studied [2]. To name a few examples, studies have considered shiftable loads in a microgrid with wind and PV [17], electrical storages in an island network with PV [18], hybrid energy systems with VRE, electricity generation and storage [19], and nuclear hybrid energy systems with VRE and storage, small modular reactors and gasoline production or water desalination [20].

More specifically, applications for heating, ventilation, and air conditioning (HVAC) load control have also been widely studied. Studies range from grid ancillary services [21, 22, 23] to economic energy management [24, 25] both in commercial and residential buildings. HVAC control with VRE at building or microgrid level has been studied by several authors. A laboratory test has been performed with a heat pump and TES in a net-ZEB with VRE [26]. Cost-optimal and rule-based control of a heat pump with TES and stationary batteries and shiftable loads has been studied [27]. Heat pump control in a dwelling with PV, TES and a PEV charged overnight has been studied [28]. Flexibility of a net-ZEB with PV, a heat pump and TES has been quantified with rule-based controls [29]. Use of building thermal mass as a buffer for voltage control with high PV penetration has been demonstrated [30]. Optimal control of a residential energy system including PV a heat pump and TES has been studied, including stochastic optimization with uncertain weather data [31]. A model predictive controller has been presented for HVAC, electricity storage and a distributed generator with PV in a residential building [32]. Optimal control and sizing of a heat pump, electric boiler and TES with PV has been studied [33]. Operation of HVAC, shiftable loads, and a battery has been optimized with PV [34]. Simulations with rule-based control of heat pumps and TES in building cooling with PV have been conducted [35]. TES has been studied as a power sink for excess PV production with a heat pump or electric boiler [36]. The operation of batteries and cooling with TES has been optimized in an office building with PV, taking forecast error into account [37]. At microgrid scale, HVAC load control has been studied with stationary electric storage in a 3-building microgrid [38], and with shiftable loads in a 1000-resident microgrid with PV and wind [39]. Optimal sizing and operation of a microgrid consisting of service and residential buildings including PV, wind, electric boiler and TES has been studied [40]. TES in DHW consumption has been studied with rule-based control in a 33-dwelling neighborhood [41].

Studies on the various applications of PEV smart charging are also numerous and include wind [42, 43] and PV [44] integration on a national scale, as well as providing grid ancillary services using thousands of PEVs [45, 46]. VRE integration using PEVs has been studied by Honarmand et al. [47] in a microgrid with also micro-turbines and fuel cells, reducing the permitted cycling of older PEV batteries to prevent battery degradation. PEV smart charging has been studied in combination with stationary batteries with VRE in commercial microgrids,

without explicitly modeling battery wear or thermal dynamics [48, 49]. VRE integration and energy management of PEVs in a MG has also been studied by Su et al. [50], using two-stage stochastic optimization to account for the VRE uncertainty. Stochastic coordination of PEVs with wind power in a MG has also been studied [51], with only SOC limits for the battery. PEV smart charging and stationary batteries have also been studied in a single household with PV, without modeling battery wear [52]. Optimal energy management in a single household with PEV smart charging and VRE generation has also been studied, including simple battery wear cost calculations for the PEVs [53, 54]. Ouammi [55] studied a MG with PEVs, electric energy storage and micro-CHP (combined heat and power), without direct modeling of battery degradation. PHEVs with micro-CHP and TES have also been studied with probabilistic optimization, without taking battery degradation into account [56]. Demand side management in 10-household cooperatives with PEVs and shiftable loads with PV has been studied [57]. PEVs have also been studied for MG voltage balancing and frequency control with VRE in islanded operation [58].

The adverse effect of battery degradation on the economics of energy arbitrage with V2G was identified by Peterson et al. [59]. However, the battery degradation model was based on cycling at room temperature. The feasibility of V2G as a peak power resource considering battery ageing has been studied [60], taking ambient temperature into account but without any battery thermal management. A battery degradation model for PEVs neglecting battery temperature was proposed has been used for optimizing residential V2G with PV [61]. PEV optimization with PV and wind power has also been studied in a reconfigurable microgrid with a simple battery degradation model, neglecting battery temperature [62]. V2G programs have also been simulated with a battery wear model neglecting battery temperature [63]. However, battery thermal management is important for battery performance and lifetime, and ambient temperature has significant impact on PEV utility [64, 65, 66].

While many studies dedicated to SHLC model building thermal dynamics and the HVAC systems in more detail and with greater time resolution than the proposed model, they do not consider PEV smart charging and often span a limited time period, less than a year. Household energy management studies including PEV smart charging on the other hand often either omit SHLC entirely, or account for it approximately without considering the actual thermal dynamics of the houses. Similarly, the effect of battery and ambient temperatures on the PEV utility and battery degradation are often neglected. Scalability of the benefits gained by aggregating multiple households together to a cooperative community has been studied with shiftable loads [67] and stationary batteries with micro-CHP and thermal energy storage [68], additionally with air conditioning [69]. Aggregating office buildings with controlled air conditioning has also been studied [70, 71]. However, the benefits of aggregation in a residential microgrid have not been studied with PEVs or SHLC.

The new contributions of this work can thus be summarized as follows:

- Combining SC/V2G and SHLC technologies modelled with thermal dy-

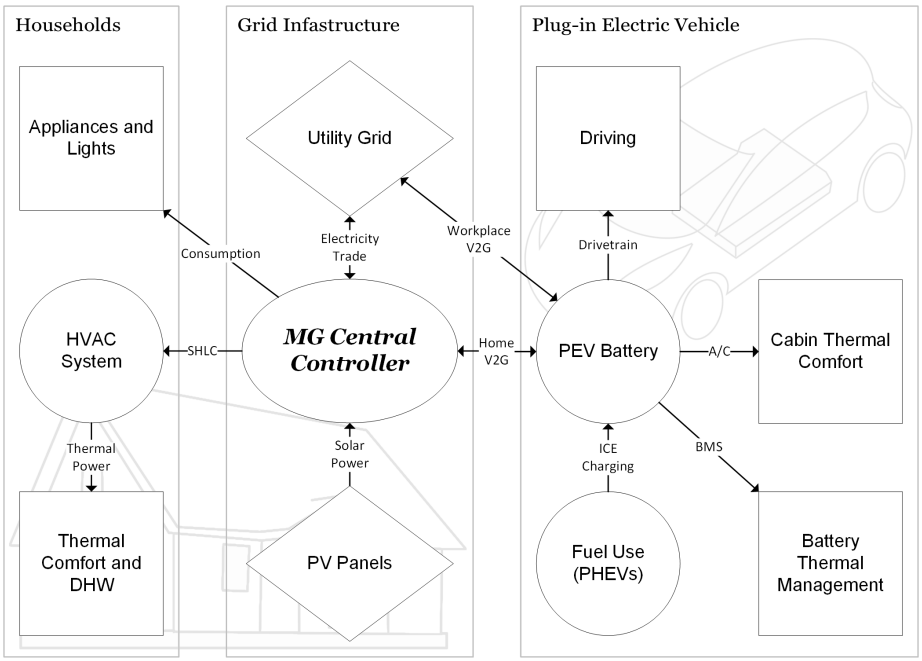

Figure 1: The energy flows within the modelled microgrid (MG). The circles represent controllable devices, the diamonds represent electricity infrastructure, and the squares represent required uses for energy in the MG.

namics.

- Modelling of the PEV utility and battery degradation, accounting for the varying usage and temperatures.
- Cost-optimal control in net-ZEBs with PV with hourly time resolution spanning an entire year.
- Scalability of the benefits of a centrally managed residential smart neighborhood with these technologies.

2. Energy management model, optimal control method and data

The modelled microgrid (MG) consists of a number of households ranging from 1–10 with one PEV in each household. Figure 1 presents an illustration of the energy flows within the modelled MG, where the house heating and cooling systems and the PEVs are treated as controllable loads capable of scheduling their behaviour according to the requirements of the MG central controller.

2.1. Space heating

The detached houses are modeled with a thermal two-capacity model for simplicity and computational efficiency, illustrated in Figure 2. The two-capacity

model can predict indoor temperature dynamics with a reasonable accuracy [72]. The concrete slab floor contains most of the heat capacity of typical single-family houses in southern Sweden [73], hence the rather light, wooden other parts of the envelope are lumped to the indoor air node. The houses are assumed to be rectangular and single-storey, as well as to have plinth foundations [74], allowing us to use the same external temperature time series for the heat losses through the floor as through the rest of the house exterior. The houses in the MG are modelled to have hydronic radiator or floor heating systems with a GSHP used for both heating and cooling, as illustrated in Figure 3. The GSHP is employed for energy-efficient electric heating and cooling: it is set up in variable condensing and provides ground source free cooling. This way, space heating, cooling and DHW are all provided efficiently.

The energy balances of the two-capacity model are given by

$$C_i \frac{dT_i}{dt} = \Phi_i^{\pm} + H_{ie}(T_e - T_i) + H_{if}(T_f - T_i), \tag{1}$$

$$C_f \frac{dT_f}{dt} = \Phi_f^{\pm} + H_{fe}(T_e - T_f) + H_{if}(T_i - T_f). \tag{2}$$

C are the heat capacities and T the temperatures of the interior (i), floor (f), and ambient air (e) nodes. H are the heat transfer coefficients between the

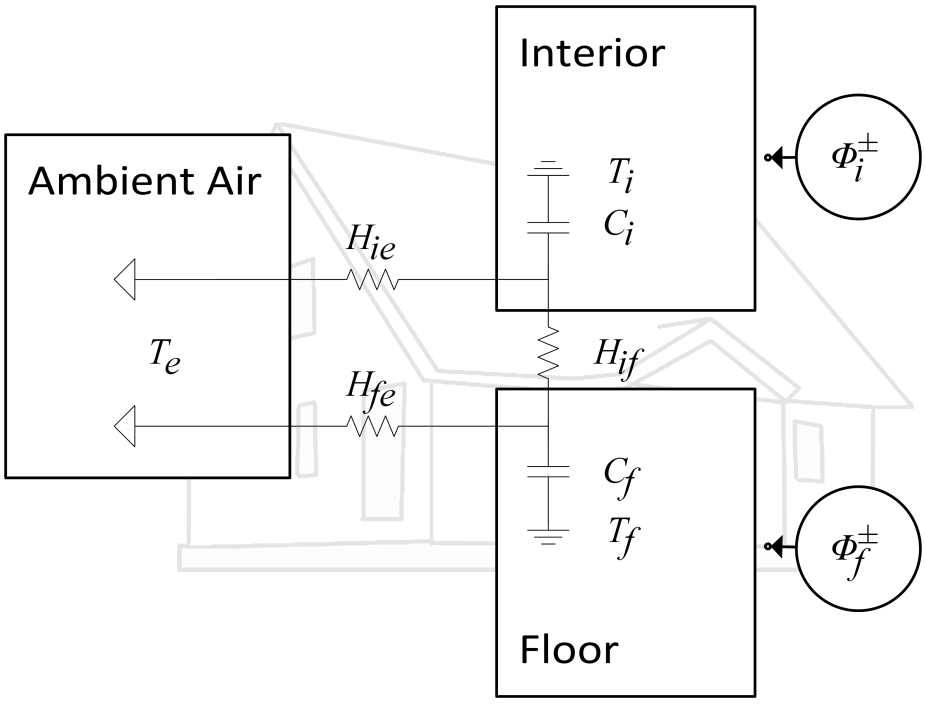

Figure 2: The detached house thermal model.

nodes, and $\Phi^{\pm}$ are the heat powers to/from each node from heating/cooling:

$$\Phi_i^{\pm} = P_{app,h,t} + \varphi_{ppl,h,t} + \varphi_{sol,h,t} + \alpha_{h,t}^{+}\psi_{h,t}^{+} - \alpha_h^{-}\psi_{h,t}^{-}, \tag{3}$$

$$\Phi_f^{\pm} = 0. \tag{4}$$

$\psi_{h,t}^{+}$ and $\psi_{h,t}^{-}$ are the heating (+) and cooling (−) equipment electric power draws respectively, $\alpha_{h,t}^{+}$ and α_h^{-} the corresponding coefficients of performance (COP), and $P_{app,h,t}$, $\varphi_{ppl,h,t}$ and $\varphi_{sol,h,t}$ are the passive heat gains from appliances (*app*), inhabitants (*ppl*), and solar radiation (*sol*) respectively. The powers in Eq. (3)–(4) are for radiator heating systems; for floor heating systems, $\alpha_{h,t}^{+}\psi_{h,t}^{+}$ is applied to the floor node instead of the interior node. Cooling is provided to the interior node regardless of the heating system. Assuming constant powers $\Phi^{\pm}$ over the simulation time step, the differential equation system is linear and can be solved analytically. See Supplementary Information for the solution.

The appliance and lighting electricity consumption time series $P_{app,h,t}$ are from an empirical measurement campaign in Sweden [75], see Supplementary

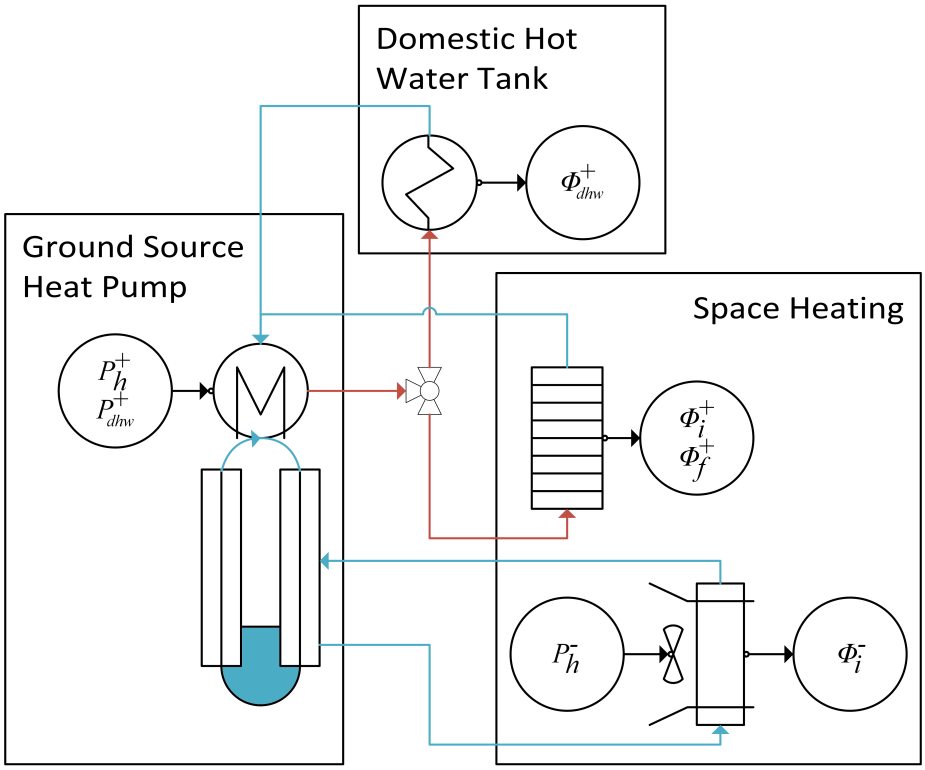

Figure 3: The modeled hydronic heating system with a ground source heat pump for both space and DHW heating. Cooling is done by ground source free cooling, i.e. circulating heat-transfer fluid from the borehole through heat exchangers in the ventilation.

Information for details. The passive heating power of the residents $\varphi_{ppl,h,t}$ is calculated based on a typical Swedish daily schedule from 1990/91 [76] and average heat gains of the different activities [77]. Newer statistics from 2010/11 [78] don't present an applicable average daily schedule, but show no changes from the 1990/91 survey that are significant at an hourly time resolution. The passive solar heat gains $\varphi_{sol,h,t}$ were calculated with ALLSOL [79] with solar radiation data from the Norrköping-SMHI weather station (59°N, 16°E) [80].

The parameters of the building envelopes are from TABULA building typology for Sweden [73]. Parameters corresponding to advanced refurbishment for energy efficiency have been used. See Supplementary Information for details on the building and heating system models.

The temperatures and electric powers are constrained to enforce strict thermal comfort of the occupants and maximum power of heating and cooling devices:

$$T_{min,i} \leq T_{i,h,t} \leq T_{max,i} \qquad \forall\, h,t, \tag{5}$$

$$T_{min,f} \leq T_{f,h,t} \leq T_{max,f} \qquad \forall\, h,t, \tag{6}$$

$$0 \leq \psi^{+}_{h,t} \leq \psi^{+}_{max,h,t} - \psi_{dhw,h,t} \qquad \forall\, h,t, \tag{7}$$

$$0 \leq \psi^{-}_{h,t} \leq \psi^{-}_{max,h} \qquad \forall\, h,t. \tag{8}$$

The floor node temperatures are constrained between 19 and 29 °C according to thermal comfort standards [81], and the interior node temperatures between 20 and 22 °C [75]. The term $\psi_{dhw,h,t}$ is the electricity consumption of heating DHW with the heat pump. The DHW tank is not used for flexibility in the model, and essentially only affects the maximum controllable power of the heat pump (see Supplementary Information for details).

2.2. Plug-in electric vehicles

The PEV model in this work considers both regular PEVs and plug-in hybrid electric vehicles (PHEVs) with a series powertrain. The model comprises of simulation of driving schedules based on statistical data, electricity balance and thermal models of the vehicle and battery, and a semi-empirical model of battery degradation. The parameters of the model are presented in Supplementary Information.

The electricity balance of a PEV is

$$\frac{dE(t)}{dt} = \eta_b \eta_c (P^{+} + \eta_F F^{+}) - P^{-} - D^{-} - \Psi^{\pm} - \nu E(t), \tag{9}$$

where ν is the self-discharge rate of the battery system [82], $E(t)$ is the energy stored in the battery of the vehicle, η_b is the battery charging and discharging efficiency, and η_c is the efficiency of the on-board battery charger. P^{+} and P^{-} are the total charging ($^{+}$) and discharging ($^{-}$) power terms respectively, η_F is the fuel-to-electricity efficiency of the internal combustion engine (ICE) and F^{+} is the fuel energy consumption term, $\Psi^{\pm}$ is the total electric power draw of the battery and cabin thermal elements, and D^{-} is the power draw

required for driving. Assuming constant powers over the simulation time step, the linear differential equation can be solved analytically (see Supplementary Information).

The thermal behavior of the vehicles is modeled using a two-capacity model similar to that of the houses, illustrated in Figure 4. The linear differential equation system is solved analytically assuming constant powers over the simulation time step (see Supplementary Information).

The battery and cabin total thermal power terms consist of separate decision variables for the electric power draws of the different thermal elements as follows:

$$\Phi^{\pm}_{b,v,t} = \alpha^{+}_{b}\eta_b\psi^{+}_{b,v,t} - \alpha^{-}_{b}\eta_b\psi^{-}_{b,v,t} \qquad \forall\, v,t, \tag{10}$$

$$\Phi^{\pm}_{c,v,t} = \alpha^{+}_{c}\eta_b\psi^{+}_{c,v,t} - \alpha^{-}_{c}\eta_b\psi^{-}_{c,v,t} \qquad \forall\, v,t, \tag{11}$$

where α^{+}_{b}, α^{-}_{b}, α^{+}_{c} and α^{-}_{c} are the COPs for the heating ($^{+}$) and cooling ($^{-}$) elements of the battery ($_b$) and cabin ($_c$) thermal systems, and $\psi^{+}_{b,v,t}$, $\psi^{-}_{b,v,t}$, $\psi^{+}_{c,v,t}$ and $\psi^{-}_{c,v,t}$ are the corresponding electric power draws. The total electric power draw of the battery and cabin thermal elements is calculated simply as

$$\Psi^{\pm}_{v,t} = \psi^{+}_{b,v,t} + \psi^{-}_{b,v,t} + \psi^{+}_{c,v,t} + \psi^{-}_{c,v,t} \qquad \forall\, v,t. \tag{12}$$

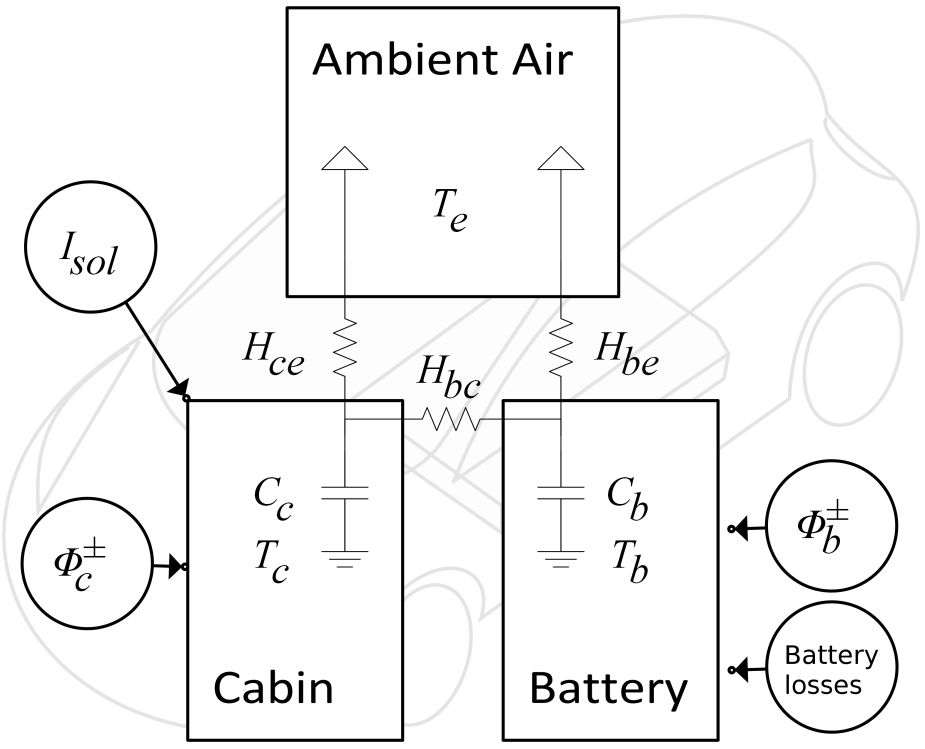

Figure 4: The two-capacity PEV thermal model.

The thermal modeling of the vehicles is based on previous studies [64, 65], and the values of the thermal parameters are based on [83].

The driving patterns that determine the driving consumption $D^-_{v,t}$ are generated using inverse transform sampling of cumulative distribution functions based on Swedish travel survey statistics [84]. See Supplementary Information for details.

Experimental data related to the technical specifications and driving consumptions of the modeled vehicles were obtained from [85]. The energy consumption of the drivetrain $D^-_{v,t}$ is assumed to be independent of the ambient temperature, and is calculated by multiplying the distances driven, as determined by the generated driving patterns, with the average energy consumption per kilometre of the vehicle. The used values have been measured at 23°C with air conditioning off for the urban dynamometer driving schedule [85]. The increased energy consumption while driving in cold or hot ambient temperatures is thus only accounted for by the cabin and battery thermal management systems.

The constraints for the PEV decision variables are presented in Table 1, where SOC_{min} and SOC_{max} are the minimum and maximum permitted states of charge (SOC) of the PEV batteries, $L_{v,t}$ is the cumulative battery degradation ratio, $g_{v,t}$ is a binary time series indicating whether vehicle v is grid-connected on hour t, $w_{v,t}$ is a binary time series indicating whether the vehicle is located at the workplace charging station, and h_v is a binary coefficient corresponding to whether vehicle v is a hybrid. y is a binary constant that indicates whether an electricity transmission agreement from the MG to workplace is in place. In order to correctly account for the interactions between the PEV, the MG and the utility grid, the total charging and discharging power terms are separated

Table 1: PEV constraints, valid for all vehicles v and time steps t.

Battery SOC with capacity fade ratio $L_{v,t}$	$SOC_{min}(1-L_{v,t})E_{max,v,0} \leq E_{v,t} \leq SOC_{max}(1-L_{v,t})E_{max,v,0}$	(13)
Battery temperature	$T_{min,b} \leq T_{b,v,t} \leq T_{max,b}$	(14)
Cabin temperature when driving	$T_{min,c} \leq T_{c,v,t} \leq T_{max,c}, \quad \text{if } D^-_{v,t} > 0$	(15)
Electric power of battery and cabin heating and cooling devices	$0 \leq \psi^+_{c,v,t} \leq \psi^+_{max,c,v}$	(16)
	$0 \leq \psi^-_{c,v,t} \leq \psi^-_{max,c,v}$	(17)
	$0 \leq \psi^+_{b,v,t} \leq \psi^+_{max,b,v}$	(18)
	$0 \leq \psi^-_{b,v,t} \leq \psi^-_{max,b,v}$	(19)
Total charging/discharging	$0 \leq P^+_{v,t} \leq g_{v,t}P^{\pm}_{max,v}$	(20)
	$0 \leq P^-_{v,t} \leq g_{v,t}P^{\pm}_{max,v}$	(21)
Charging/discharging in the MG	$0 \leq S^+_{v,t} \leq (yw_{v,t} + (1-w_{v,t})g_{v,t})P^{\pm}_{max,v}$	(22)
	$0 \leq S^-_{v,t} \leq (yw_{v,t} + (1-w_{v,t})g_{v,t})P^{\pm}_{max,v}$	(23)
Charging/discharging at the workplace	$0 \leq G^+_{v,t} \leq w_{v,t}P^{\pm}_{max,v}$	(24)
	$0 \leq G^-_{v,t} \leq w_{v,t}P^{\pm}_{max,v}$	(25)
ICE power for PHEVs	$0 \leq F^+_{v,t} \leq h_v F^+_{max,v}$	(26)

into further decision variables as

$$P^+_{v,t} = S^+_{v,t} + G^+_{v,t} \qquad \forall\, v, t, \tag{27}$$

$$P^-_{v,t} = S^-_{v,t} + G^-_{v,t} \qquad \forall\, v, t, \tag{28}$$

where $S^+_{v,t}$ and $S^-_{v,t}$ are charging and discharging terms between the PEV and the MG, and $G^+_{v,t}$ and $G^-_{v,t}$ the corresponding terms between the PEV and the utility grid.

A PHEV duty cycle ageing model for 3.75 V, 15 Ah pouch NMC-LMO/graphite cells [86] is employed for battery degradation. Blending NMC to LMO cathodes combines the benefits of the two materials, increasing e.g. cycle life compared to LMO [86]. The two vehicles modeled directly in this work, Nissan Leaf and Chevrolet Volt, have LMO cathodes in their batteries [85], and have also been reported to adopt NMC-LMO blended cathodes [87, 88, 89]. Other models for estimating the battery state-of-health have also been presented, e.g. [90].

The model [86] describes the total capacity fade percentage of a cell due to cumulative Ah-throughput J. To allow for variable temperature in our model, we formulate it in terms of additional capacity fade on simulation time step t, with $L_{v,t}$ indicating the total capacity fade ratio:

$$L_{v,t+1} = L_{v,t} + \frac{1}{100} a_c \exp\left(-\frac{2E_{ac}}{R_g(T_{b,v,t+1} + T_{b,v,t})}\right)(J^z_{v,t+1} - J^z_{v,t}), \tag{29}$$

where

$$a_c = \alpha_c + \beta_c r^b + \gamma_c (SOC_{min} - SOC_0)^c. \tag{30}$$

The terms α_c, β_c, b, γ_c, SOC_0, c, and z are dimensionless constants used in fitting the model, E_{ac} is the cell activation energy for the capacity fade process, R_g is the universal gas constant, J_t is the Ah throughput of a cell in the battery system, and r is a parameter that determines whether the vehicle is driven in charge-depleting or charge-sustaining mode. For simplicity, the PHEVs are assumed to always operate in charge-depleting mode. This is a good approximation, as the ICE share of PHEV electricity is only in the order of 1% with the studied controls. The cell temperature is averaged over two subsequent time steps in order to smooth the effects of the hourly time step, limited by data availability.

The Ah throughput of a cell J_t is approximated as

$$J_{v,t} \approx \frac{Q_{cell}}{Q_{system}} \frac{\Delta t}{U} \sum_{k=1}^{t} \left[\eta_c (P^+_{v,k} + \eta_F F^+_{v,k}) + P^-_{v,k} + D^-_{v,k} + \Psi^{\pm}_{v,k}\right], \tag{31}$$

where U is the nominal voltage of the battery system, and Q_{cell} and Q_{system} are the rated Ah capacities of the individual battery cell and the battery system, respectively. An ideal battery pack is assumed: all the cells are drained equally and their temperatures are equal.

The marginal cost due to degradation of operating the battery in €/Wh is obtained by differentiation of the degradation model [86] with respect to J, converting Ah units to Wh with the nominal voltage approximation, and multiplying with cost of Wh capacity p_b.

$$p_{d,v,t} = p_b \frac{E_{max,v,0}}{U} \frac{Q_{cell}}{Q_{system}} \frac{1}{100} z a_c \exp\left(-\frac{2E_{ac}}{R_g(T_{b,v,t+1} + T_{b,v,t})}\right) J_{v,t}^{z-1}. \quad (32)$$

The cost is a decreasing function of the cumulative Ah throughput $J_{v,t}$, as $z = 0.48$ [86].

Since the battery degradation model in Eq. (29) is nonlinear, it cannot be explicitly included in the LP model. However, because battery degradation is a rather slow cumulative process, we can include it iteratively without causing a significant error as follows:

1. Calculate the initial battery degradation time series $L_{v,t}$ with an initial guess of PEV usage.
2. Perform the LP optimization using $L_{v,t}$ to constrain the battery SOC.
3. Calculate a new $L'_{v,t}$ using the optimized PEV usage.
4. Perform the LP optimization using $L'_{v,t}$ to constrain the battery SOC.
5. Repeat steps 3 and 4 until convergence or for a predetermined number of iterations.
6. Calculate the final $L''_{v,t}$ based on the latest optimization results.

Iterating the battery degradation in this manner only seems to reach convergence with a maximum of three PEVs, probably because with multiple PEVs the LP optimization can alternate between them based on which one has the least strict SOC constraints. However, even with only a few iterations the mismatch between the PEV battery SOCs and the battery degradation becomes reasonably small. Three iterations were used for the results presented in this work, resulting in total excess of PEV battery capacity in the order of 1 % of total PEV charge or less. The optimal controls use the corresponding baseline PEV use as the initial guess; for the baseline simulations, the initial guess is zero use.

2.3. Microgrid energy balance, objective functions and solution scheme

The microgrid (MG) electricity balance is set by the equality constraint

$$\begin{aligned} \sum_v [S^+_{v,t} - \eta_b \eta_c S^-_{v,t}] + \sum_h [\psi^+_{h,t} + \psi^-_{h,t}] + G_{s,t} - G_{b,t} \\ = -\sum_h [P_{app,h,t} + \psi_{dhw,h,t}] + P_{sol,t} \end{aligned} \qquad \forall\, t, \quad (33)$$

where the grid connection variables for buying electricity from the utility grid to the MG $G_{b,t}$ and selling excess electricity from the MG into the utility grid $G_{s,t}$ are constrained according to

$$0 \le G_{s,t} \le G_{max} \qquad \forall\, t, \quad (34)$$

$$0 \le G_{b,t} \le G_{max} \qquad \forall\, t. \quad (35)$$

The maximum power capacity of the connection between the MG and the utility grid G_{max} is scaled based on the number of modelled households N_h in the MG as

$$G_{max} = 24\, N_h \text{ kW}. \tag{36}$$

The 24-kW connection capacity per household corresponds to three-phase power with 35-A main fuses and a phase voltage of 230 V.

The residential MG sells electricity at the hourly day-ahead market spot price $p_{m,t}$ [91], buys electricity at the retail price $p_{r,t}$, and pays $p_{F,t}$ for electricity from PHEV combustion engines. All energy throughput of the battery incurs battery degradation cost p_d. The objective function used in this work is a total cost minimizing function

$$\begin{aligned} f_{cost} = \sum_t \Big\{ \sum_v \big[&(p_{r,t} + p_{d,v,t}) G^+_{v,t} - (\eta_c \eta_b p_{m,t} - p_{d,v,t}) G^-_{v,t} \\ &+ (p_{F,t} + p_{d,v,t}) F^+_{v,t} + (p_{d,v,t} + p_f w_{v,t})(S^+_{v,t} + \eta_c \eta_b S^-_{v,t}) + p_{d,v,t} \Psi^{\pm}_{v,t} \big] \\ &+ p_{r,t} G_{b,t} - p_{m,t} G_{s,t} \Big\}. \end{aligned} \tag{37}$$

The additional fees p_f include distribution cost and electricity tax, and apply on top of the day-ahead market price in the retail price

$$p_{r,t} = 1.25 \times (p_{m,t} + p_f), \qquad \forall t, \tag{38}$$

where the multiplier of 1.25 accounts for value-added tax [91]. The same fees p_f are applied to transmission of power between the MG and the PEV when the PEV is at work, as determined by the time series $w_{v,t}$.

Hourly electricity day-ahead market prices for Sweden in 2005–2006 used in this work were obtained from Nord Pool Spot [92]. Fuel price data was obtained from the Weekly Oil Bulletin statistics by the European Energy Commission [93]. The fuel prices used in this work are tax-inclusive EU weighted weekly average prices of Euro-Super 95 petrol from 2005–2006, which were linearly interpolated to daily values that change at midnight, as is typical for gasoline stations. The energy content in the fuel is calculated with a typical energy density of gasohol E10 of about 9.2 kWh/l [94], and the PHEV ICEs are assumed to have 30% energy conversion efficiency [95]. Electricity produced by the ICE costs around 4 times the retail price of electricity.

The optimized scheduling of the PEVs and the HVAC systems is compared against a baseline scenario where PEV charging and HVAC systems are optimized separately to minimize their energy consumption. This way, the comparison shows the effect of flexibility in the cost-optimization, without significant additional energy efficiency gains. Gains compared to conventional thermostat controls could be higher.

The baseline PEV charging schedule is calculated by minimizing the usage of the battery

$$f_{PEV} = \sum_t \sum_v \left[-0.1 E_{v,t} + P^+_{v,t} + P^-_{v,t} + 10 F^+_{v,t} \right], \tag{39}$$

with an incentive term for keeping the batteries as full as possible and a penalty term for fuel usage. The incentive term is used to simulate range anxiety of the driver, and conventional PEV charging, which charges the battery to complete charge at full power. The fuel use is penalized since it is always more expensive to use fuel to recharge the PHEVs if electricity is available. The PEV baseline optimization with Eq. (39) only uses the PEV constraints in Eqs. (9)-(31), resulting in each PEV scheduling its charging solely according to its driving pattern.

The baseline HVAC system schedule is calculated by minimizing its electricity consumption

$$f_{HVAC} = \sum_t \sum_h \left[\psi^+_{h,t} + \psi^-_{h,t} \right], \tag{40}$$

constrained by Eqs. (1)-(8). When calculating the baseline HVAC behaviour, the interior node temperature is forced to stay at the midpoint of the allowed interval to simulate a less intelligent thermostat system.

All the optimizations in this work are conducted with the horizon of a full year from September 2005 to August 2006, assuming perfect information. The results hence represent the best possible case, or an upper limit to the achievable benefits with limited forecast horizon and accuracy in actual implementation. Analyzing the effects of forecast horizon and error with available forecasts is left for further work. Moreover, the model solves hourly energy balances, as data availability limits the time resolution to hourly. This corresponds to hourly net metering.

The optimal MG energy management problem instances were solved with CPLEX 12.4 for MATLAB on a desktop computer with an Intel Xeon E3-1230 processor and 16 GB of RAM. CPLEX uses simplex and barrier algorithms to solve linear programs [96]. The solver was allowed to select the algorithm automatically in a way that should give best overall performance. A single optimization sequence consists of optimizing the baseline PEV and space heating behaviour, and then optimizing the full MG energy management problem. All the optimizations including PEVs are also iterated three times in order to sufficiently account for the battery degradation, and the final results are then calculated based on the various optimized decision variable time series, as well as the known prices for electricity, transmission and fuel.

The costs of PEV battery degradation are included by calculating the total battery degradation over the year based on Eq. (29) for both the baseline and the cost-optimal PEV use, and then calculating the value of the lost battery capacity using p_b. The change in the cost of battery degradation in cost-optimal control vs. baseline is then added into the total electricity costs of the cost-optimal case. This way, the cost of additional battery degradation in the cost-optimal case vs. conventional PEV use in the baseline is visible in the results. The batteries are new at the start of each annual simulation, resulting in faster battery degradation than for used ones, as determined by Eq. (29). Hence, V2G becomes increasingly economical towards the end of each simulation. This is because the cost of the additional battery degradation due to

V2G becomes lower as the battery ages. This is visible in the marginal cost of battery degradation (32), which is a decreasing function of the cumulative Ah throughput.

2.4. Examined scenarios

The energy management optimizations are carried out for four different cases, representing different system infrastructures as follows:

Case I represents an individual house with PV generation and a PEV ($y = 0$).

Case II represents an individual house with PV generation, a PEV, and a hypothetical electricity transmission agreement allowing the household to transfer electricity between the home MG and the workplace charging station for a small fee ($y = 1$).

Case III represents a cooperative microgrid with PV generation consisting of 1–10 houses each with their own PEV. Electricity is transferred freely between the households, PEVs and PV panels in the microgrid, but there is no transfer to the workplace ($y = 0$).

Case IV represents the same cooperative microgrid, now with the hypothetical electricity transfer agreement ($y = 1$).

Each case is optimized for three different PEV and HVAC system combinations, representing increasing amounts of thermal and PEV battery storage capacities: radiator heating and Chevrolet Volt (floor slab thickness 8 cm), floor heating (slab thickness 8 cm) and Nissan Leaf, and floor heating with improved storage capacity (slab thickness 12 cm) and high-end BEV.

The yearly electricity consumption of the appliances and lighting in the modelled houses varies considerably between around 2.3–11.4 MWh, averaging around 5.7 MWh per year. In order to eliminate unnecessary variability in the results, the electricity consumption time series of each household are normalized to match the mean yearly electricity consumption. Similarly, each house is modeled with a floor area of 145 m^2 and 3.2 inhabitants according to the corresponding mean values of the modeled houses, in order to normalize the HVAC and DHW electricity consumptions of each house. In the cases with multiple modeled houses, the results are averaged over three different orders in which the houses are added into the MG.

Each modeled PEV is assumed to be technically identical and their driving habits are assumed to be the same. The generated driving patterns still vary considerably, resulting in yearly driven distances between 18,000 and 20,000 km per PEV, which is high compared to the average Swedish value, around 12,000–13,000 km per car per year [97]. However, this value is calculated based on Swedish road traffic statistics, and includes vehicles that are not used regularly for commuting. Again, in order to eliminate unnecessary variability the yearly kilometers driven by each PEV is normalized to 18,900 km, corresponding to the mean yearly distance driven by the PEVs with the three different driving

generator seeds used in this work. The results are averaged over the different random seeds.

The houses in each scenario are modelled as net zero energy buildings, defined [98] in terms of annual electricity balance: the yearly total PV generation equals the yearly electricity consumption of the modeled houses, including baseline HVAC consumption but excluding PEVs. This results in PV generation capacities of around 10–11 kW_p per household, slightly depending on the modeled microgrid and HVAC systems. PEV battery value of 260 €/kWh [99] and transmission fees of 50 €/MWh [91] are used.

3. Results

Figure 5 presents the yearly costs, as well as amounts of bought and sold electricity per household for the different cases for SHLC-only and V2G-only optimizations, the other flexibility source with baseline control. In the cases with 1–10 houses, the results are averaged over the different numbers of houses. V2G can achieve 104–203 € (12–20%) and SHLC 66–170 € (8–16%) yearly cost savings per household, depending on the modelled HVAC system and case. V2G provides more savings than SHLC in all configurations except cases I–III with Nissan Leaf and floor heating. V2G decreases the annual sold and bought electricity more than SHLC in all the configurations, indicating that the PEVs are more effective at increasing the self-consumption of locally produced PV electricity. This is expected, as PV generation peaks during the summer, when heating demand is at its lowest. SHLC can use space cooling in the summer, but the flexible electric power in the energy-efficient ground source free cooling is only around 20% that of space heating with the GSHP. Thermal storage in DHW heating [27] could increase the benefits of heating control.

Figure 6 presents the yearly costs, as well as amounts of bought and sold electricity per household for the different cases with cost-optimal control for both PEVs and SHLC. PEV charging is considered both with V2G capability and only SC. In the cases with 1–10 houses, the results are averaged over the different numbers of houses. The yearly savings per household achieved with V2G and SHLC range from 167 € to 340 € (19–33%), depending on the modelled PEVs and HVAC systems. However, the additional cost savings of V2G compared to SC are minor: 4–8 € per household annually, or less than 1 percentage point. V2G provides a considerable increase in self-consumption of the locally produced PV electricity, as observed in the decrease in bought and sold electricity. With the studied prices, this increase in self-sufficiency does not translate to significant cost savings: the benefit of the additional self-consumption is low compared to the cost of additional battery degradation. Similarly, aggregating multiple households or permitting electricity transmission between the home MG and a workplace charging station (cases II-IV) provide significant decrease in bought and sold electricity, but the resulting cost savings are limited.

Sensitivity of the V2G results to battery cost and degradation was studied by running the optimizations at different battery costs, conducting the optimizations without battery degradation but taking it into account in the simulations,

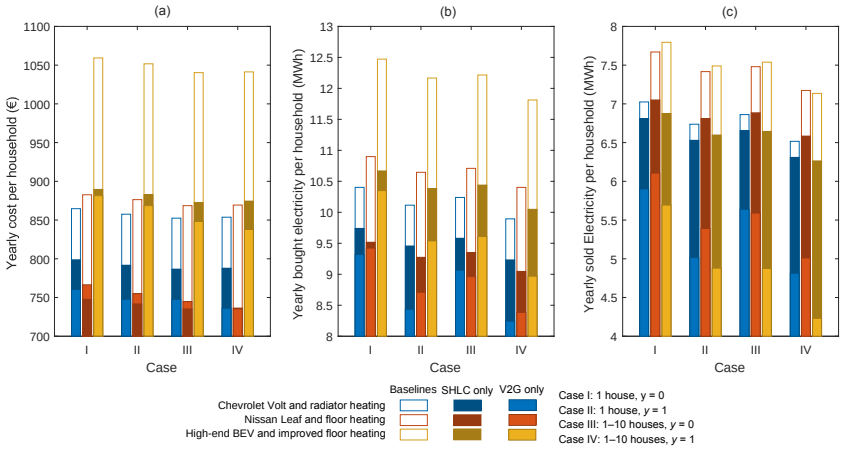

Figure 5: Yearly costs of electricity (a), and bought (b) and sold (c) amounts of electricity per household for the examined cases with only V2G or SHLC optimized, with baseline control for the other resource.

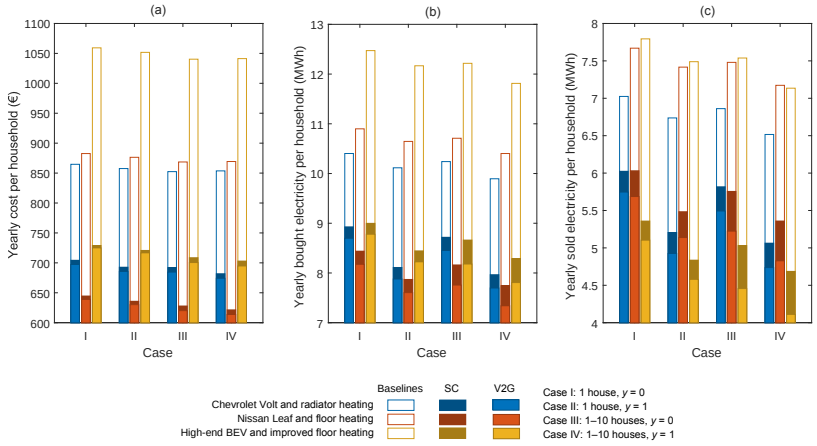

Figure 6: Yearly costs of electricity (a), and bought (b) and sold (c) amounts of electricity per household for the V2G-capable and SC-only optimizations.

and neglecting battery degradation completely. These runs were done with only one order of adding the houses to the MG, as well as with only one driving generator seed.

V2G use is sensitive to increase in the battery cost. Increasing the battery cost from 260 €/kWh to 360 €/kWh [99] causes the high-end BEV to stop

using V2G in addition to SC almost completely, and Nissan Leaf to significantly decrease its V2G use.

V2G is also used excessively in many system configurations if the optimizations are performed without including the estimated cost of battery degradation $p_{d,v,t}$ (Eq. (32)), but the degradation is included in the simulations and the resulting cost is incurred in the final cost. This simulates real-life optimal control without taking battery degradation into account. The excessive V2G use often leads to increase in total cost. When V2G can provide cost benefit compared to SC, it remains limited: 1 percentage point or less. The effects of degradation cost are the most pronounced with the high-end BEV as the degradation cost for given Ah throughput scales with the number of cells in the battery system (Eq. (32)) With the high-end BEV and transmission to workplace, the V2G-capable solution is more expensive per household than the SC-only solution already with the battery value of 260 €/kWh, if both are optimized unaware of the degradation cost. With Nissan Leaf optimized this way, V2G remains slightly less expensive than SC; with Chevrolet Volt, V2G becomes more expensive than SC with the flexibility offered by 5 or more houses and transmission to workplace. Increasing the battery cost to 360 €/kWh [99], only Chevrolet Volt without transmission to workplace and Nissan Leaf with one house and transmission to workplace can provide cost decrease with V2G compared to SC. At battery cost 450 €/kWh [99], only Chevrolet Volt with 1 or 3 houses and without workplace transmission can benefit from V2G costwise.

If battery degradation is neglected completely in the model, the results indicate that V2G would provide 2–5 percentage points of cost benefit compared to SC. This shows that neglecting battery degradation can lead to overestimating the cost benefit of V2G, as the additional benefit compared to SC is less than 1 percentage point or even negative if battery degradation is considered. However, new batteries have been used in the simulations, and the degradation slows down and V2G becomes more economical as degradation proceeds (Eqs. (29) and (32)). Degradation could hence hinder the economics of V2G less over the whole life of the vehicle, and V2G with used batteries would be an especially interesting option.

The benefits gained per household when the size of the microgrid is increased are limited, as seen from Figure 7. Results for case IV with V2G are presented, but they are similar for cases III and IV with V2G or only SC. Depending on the modeled PEV and HVAC systems, the additional decrease in yearly costs, as well as bought and sold electricity is only around 1–6 percentage points, with saturation at 3–5 households. However, since the current model operates on perfect information, it is possible that aggregating multiple households could help to reduce the effects of uncertainty in real-life applications. Moreover, the houses considered here are normalized to a large degree, and the driving of the PEVs follows the same probability distribution. Variability among the households could provide more benefits from aggregation in an actual implementation.

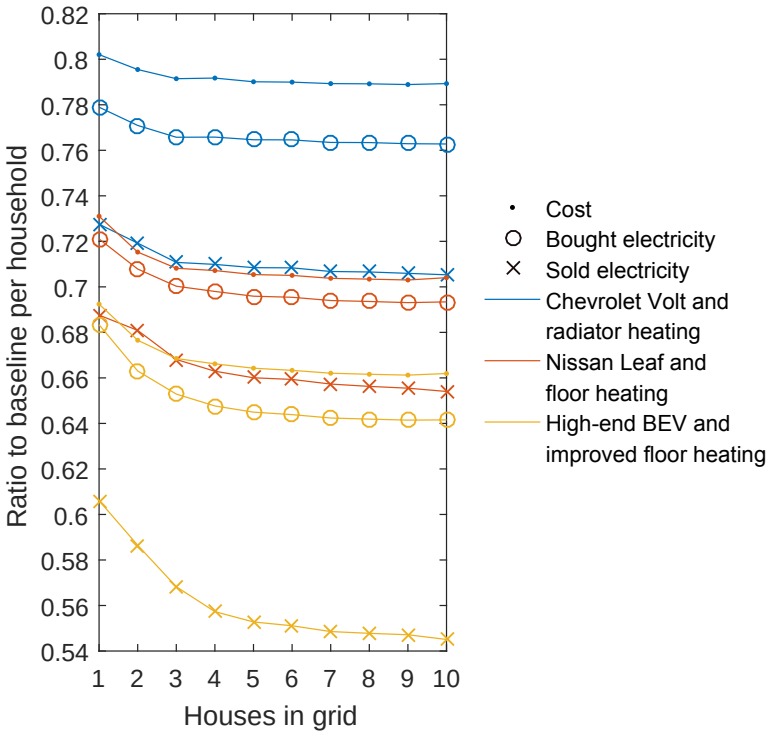

Figure 7: The ratio between the cost-optimized yearly results per household and the baseline results of an individual household as a function of the number of aggregated households in the modeled microgrid. The results are for case IV with V2G.

4. Conclusions

A physically realistic linear programming (LP) energy management model has been presented for optimizing smart charging (SC) and vehicle-to-grid (V2G), and space heating load control (SHLC) in a residential microgrid with on-site PV generation. The model includes the thermal dynamics of the modelled houses and the plug-in electric vehicles (PEV) explicitly, and capacity fade of the PEV batteries. Energy-efficient space heating and cooling with ground-source heat pumps (GSHP) and ground source free cooling is modeled. The model is generic and applicable for any conditions.

A case study was conducted with the model on a a 1–10-household hypothetical microgrid (MG) in Norrköping, Sweden, with detailed empirical data. The temperature dependence of PEV utility is especially important in the cold

climate conditions considered here. PV was dimensioned at 10–11 kW per house to obtain net zero energy houses excluding PEV use. Three PEV–space heating combinations were considered, with battery capacities from 16.5 to 70 kWh per vehicle and increasingly heavy building envelopes.

Significant annual cost savings up to 33% compared to benchmark control were found from cost-optimal control of PEVs and space heating. The benchmark control minimizes the total electricity consumption of space heating and charging and discharging of the PEVs, including incentive terms to simulate conventional PEV charging to full battery capacity, and to minimize expensive fuel use of PHEVs. V2G-capable PEVs were found to offer more flexibility to a residential MG than SHLC systems in terms of yearly cost savings in most system configurations (12–20% and 8–16%, respectively), as well as reducing the yearly amounts of sold and bought electricity. This is expected with a PV installation, as PV production is concentrated to summertime when the demand for space heating and cooling electricity is low with the studied heating system with energy-efficient ground source free cooling.

The added value of V2G compared to only SC in PEVs was found limited, less than 1 percentage point of cost savings. The cost of additional battery degradation decreases the benefit of V2G compared to SC. Moreover, cost-optimizing V2G use without accounting for the costs of battery degradation resulted in excessive V2G use in many system configurations, yielding higher annual cost than only SC. Neglecting battery degradation completely led to overestimating the cost benefit of V2G compared to SC at 2–5 percentage points. These results highlight the importance of taking the additional battery degradation into account in V2G schemes. However, old batteries degrade slower than the new batteries used in the simulations, and considering the whole vehicle life or using old batteries for V2G could make V2G more economical, especially in e.g. reserve markets where flexibility is more valuable than in the day-ahead market considered here.

The cost and energy balance benefits gained by aggregating multiple households into a small centrally managed smart grid were limited. Considering all the extra complexity of centrally managing multiple households, independently managing each household would be preferable from a customer's point of view. Similarly, the possibility to transfer excess PV generation from the home MG to the workplace PEV charging station only yielded negligible monetary savings with the considered prices, even though the self-consumption was noticeably increased.

The results indicate that significant benefits both in terms of cost and grid interaction are available through optimal control of PEVs and energy-efficient space heating in net zero energy houses powered with PV. As the optimizations were done over a whole year with perfect information, further work should study the effect of forecasts with limited horizon and accuracy. Aggregating households could be useful due to limited accuracy of single-household forecasts [100], as well as to achieve sufficient scale for direct market participation or operating in islanded mode during disturbances. The fully cooperative MG studied here may not be realistic due to conflicting single-household and MG

interests, and a more realistic business model could be e.g. based on advanced metering schemes [101].

Separate thermal energy storage (TES) could significantly increase heating flexibility, especially in the summertime with DHW demand. The nonlinear heat pump COP could be included to the optimization with TES with e.g. piecewise linearisation and mixed-integer linear programming (MILP). V2G could be more economical with old batteries that degrade slower than the new ones used in this work, especially in e.g. reserve markets where flexibility has higher value than in the day-ahead market. Avoiding high SOC values to enhance battery lifetime [13] could make SC and V2G more beneficial.

The model could be extended to cover also power fade of batteries [86] if sub-hourly data was available. The accuracy of vehicle consumption modeling could be enhanced to include driving style [65] with more detailed driving data. PEV-specific driving pattern data would also be interesting. Modeling battery operation at low temperature would be especially interesting for the cold climate conditions in this study.

Acknowledgements

This research was funded from the Academy of Finland project CONICYT (26975), and the TEKES project FLEXe (2115783).

References

[1] J. Klimstra, Power Supply Challenges - Solutions for Integrating Renewables, Wärtsilä Finland Oy, 2014.

[2] P. D. Lund, J. Lindgren, J. Mikkola, J. Salpakari, Review of energy system flexibility measures to enable high levels of variable renewable electricity, Renewable and Sustainable Energy Reviews 45 (2015) 785–807. doi:10.1016/j.rser.2015.01.057.

[3] IEA, Energy Technology Perspectives 2015, OECD/IEA, 2015.

[4] P. Bayer, D. Saner, S. Bolay, L. Rybach, P. Blum, Greenhouse gas emission savings of ground source heat pump systems in Europe: A review, Renewable and Sustainable Energy Reviews 16 (2) (2012) 1256–1267. doi:10.1016/j.rser.2011.09.027.

[5] European Heat Pump Association, European Heat Pump Market and Statistics Report 2015. Executive Summary (2015).

[6] A. Arteconi, N. Hewitt, F. Polonara, State of the art of thermal storage for demand-side management, Applied Energy 93 (2012) 371–389. URL http://linkinghub.elsevier.com/retrieve/pii/S0306261911008415

[7] A. Ajanovic, The future of electric vehicles: Prospects and impediments, Wiley Interdisciplinary Reviews: Energy and Environment 4 (6) (2015) 521–536. doi:10.1002/wene.160.

[8] M. D. Galus, M. G. Vayá, T. Krause, G. Andersson, The role of electric vehicles in smart grids, Wiley Interdisciplinary Reviews: Energy and Environment 2 (4) (2013) 384–400. doi:10.1002/wene.56.

[9] S. Rahman, G. B. Shrestha, Investigation into the impact of electric vehicle load on the electric utility distribution system, IEEE Transactions on Power Delivery 8 (2) (1993) 591–597. doi:10.1109/61.216865.

[10] K. Clement-Nyns, E. Haesen, J. Driesen, The impact of Charging plug-in hybrid electric vehicles on a residential distribution grid, IEEE Transactions on Power Systems 25 (1) (2010) 371–380. doi:10.1109/TPWRS.2009.2036481.

[11] P. Finn, C. Fitzpatrick, D. Connolly, Demand side management of electric car charging: Benefits for consumer and grid, Energy 42 (1) (2012) 358–363. doi:10.1016/j.energy.2012.03.042.

[12] K. Mets, T. Verschueren, W. Haerick, C. Develder, F. De Turck, Optimizing smart energy control strategies for plug-in hybrid electric vehicle charging, 2010 IEEE/IFIP Network Operations and Management Symposium Workshops (2010) 293–299doi:10.1109/NOMSW.2010.5486561.

[13] B. Lunz, Z. Yan, D. U. Gerschler, J. B.and Sauer, Influence of plug-in hybrid electric vehicle charging strategies on charging and battery degradation costs, Energy Policy 46 (2012) 511–519. doi:10.1016/j.enpol.2012.04.017.

[14] J. Bates, D. Leibling, Spaced out - perspectives on parking policy, Tech. rep., Royal Automobile Club Foundation for Motoring (Jul 2012).

[15] D. B. Richardson, Electric vehicles and the electric grid: A review of modeling approaches, Impacts, and renewable energy integration, Renewable and Sustainable Energy Reviews 19 (2013) 247–254. doi:10.1016/j.rser.2012.11.042.

[16] W. Kempton, S. E. Letendre, Electric vehicles as a new power source for electric utilities, Transportation Research Part D: Transport and Environment 2 (3) (1997) 157–175. doi:10.1016/S1361-9209(97)00001-1.

[17] G. Graditi, M. L. Di Silvestre, R. Gallea, E. R. Sanseverino, Heuristic-based shiftable loads optimal management in smart micro-grids, IEEE Transactions on Industrial Informatics 11 (1) (2015) 271–280. doi:10.1109/TII.2014.2331000.

[18] M. G. Ippolito, M. L. Di Silvestre, E. Riva Sanseverino, G. Zizzo, G. Graditi, Multi-objective optimized management of electrical energy storage systems in an islanded network with renewable energy sources under different design scenarios, Energy 64 (2014) 648–662. doi:10.1016/j.energy.2013.11.065.
URL http://dx.doi.org/10.1016/j.energy.2013.11.065

[19] J. Chen, H. E. Garcia, Economic optimization of operations for hybrid energy systems under variable markets, Applied Energy 177 (2016) 11–24. doi:10.1016/j.apenergy.2016.05.056.
URL http://dx.doi.org/10.1016/j.apenergy.2016.05.056

[20] J. Chen, H. E. Garcia, J. S. Kim, S. M. Bragg-Sitton, Operations Optimization of Nuclear Hybrid Energy Systems, Nuclear Technology 195 (2) (2016) 143–156. doi:10.13182/NT15-130.

[21] H. Hao, Y. Lin, A. S. Kowli, P. Barooah, S. Meyn, Ancillary Service to the grid through control of fans in commercial Building HVAC systems, IEEE Transactions on Smart Grid 5 (4) (2014) 2066–2074. doi:10.1109/TSG.2014.2322604.

[22] M. Sullivan, J. Bode, B. Kellow, S. Woehleke, J. Eto, Using residential AC load control in grid operations: PG&E's ancillary service pilot, IEEE Transactions on Smart Grid 4 (2) (2013) 1162–1170. doi:10.1109/TSG.2012.2233503.

[23] Y. J. Kim, E. Fuentes, L. K. Norford, Experimental study of grid frequency regulation ancillary service of a variable speed heat pump, IEEE Transactions on Power Systems 31 (4) (2016) 3090–3099. doi:10.1109/TPWRS.2015.2472497.

[24] J. Ma, S. J. Qin, T. Salsbury, Application of economic MPC to the energy and demand minimization of a commercial building, Journal of Process Control 24 (8) (2014) 1282–1291. doi:10.1016/j.jprocont.2014.06.011.

[25] M. Avci, M. Erkoc, A. Rahmani, S. Asfour, Model predictive HVAC load control in buildings using real-time electricity pricing, Energy and Buildings 60 (2013) 199–209. doi:10.1016/j.enbuild.2013.01.008.

[26] D. Vanhoudt, D. Geysen, B. Claessens, F. Leemans, L. Jespers, J. Van Bael, An actively controlled residential heat pump: Potential on peak shaving and maximization of self-consumption of renewable energy, Renewable Energy 63 (2014) 531–543. doi:10.1016/j.renene.2013.10.021.

[27] J. Salpakari, P. Lund, Optimal and rule-based control strategies for energy flexibility in buildings with PV, Applied Energy 161 (2016) 425–436. doi:10.1016/j.apenergy.2015.10.036.

[28] F. Pallonetto, S. Oxizidis, F. Milano, D. Finn, The effect of time-of-use tariffs on the demand response flexibility of an all-electric smart-grid-ready dwelling, Energy and Buildings 128 (2016) 56–67. doi:10.1016/j.enbuild.2016.06.041.
URL http://dx.doi.org/10.1016/j.enbuild.2016.06.041

[29] U. I. Dar, I. Sartori, L. Georges, V. Novakovic, Advanced control of heat pumps for improved flexibility of Net-ZEB towards the grid, Energy and Buildings 69 (2014) 74–84. doi:10.1016/j.enbuild.2013.10.019.
URL http://dx.doi.org/10.1016/j.enbuild.2013.10.019

[30] M. Wetter, M. Bonvini, T. S. Nouidui, Equation-based languages – A new paradigm for building energy modeling, simulation and optimization, Energy and Buildingsdoi:10.1016/j.enbuild.2015.10.017.
URL http://www.sciencedirect.com/science/article/pii/S0378778815303315http://www.sciencedirect.com/science/article/pii/S0378778815303315/pdfft?md5=5fee6e4f67a15bc742109dd37c0d89c8{&}pid=1-s2.0-S0378778815303315-main.pdf

[31] D. Lauinger, P. Caliandro, J. Van herle, D. Kuhn, A linear programming approach to the optimization of residential energy systems, Journal of Energy Storage 7 (2016) 24–37. doi:http://dx.doi.org/10.1016/j.est.2016.04.009.
URL http://www.sciencedirect.com/science/article/pii/S2352152X16300585

[32] I. Sharma, J. Dong, A. A. Malikopoulos, M. Street, J. Ostrowski, T. Kuruganti, R. Jackson, A Modeling Framework for Optimal Energy Management of a Residential Building, Energy and Buildingsdoi:10.1016/j.enbuild.2016.08.009.

[33] D. Fischer, K. B. Lindberg, H. Madani, Impact of PV and variable prices on optimal system sizing for heat pumps and thermal storage, Energy & Buildings submitted (2015) 723–733. doi:10.1016/j.enbuild.2016.07.008.
URL http://dx.doi.org/10.1016/j.enbuild.2016.07.008

[34] J. Khoury, R. Mbayed, G. Salloum, E. Monmasson, Predictive demand side management of a residential house under intermittent primary energy source conditions, Energy and Buildingsdoi:10.1016/j.enbuild.2015.12.011.

[35] A. Arteconi, E. Ciarrocchi, Q. Pan, F. Carducci, G. Comodi, F. Polonara, R. Wang, Thermal energy storage coupled with PV panels for demand side management of industrial building cooling loads, Applied Energydoi:10.1016/j.apenergy.2016.01.025.
URL http://linkinghub.elsevier.com/retrieve/pii/S0306261916300058

[36] J. Hirvonen, G. Kayo, A. Hasan, K. Sirén, Zero energy level and economic potential of small-scale building-integrated PV with different heating systems in Nordic conditions, Applied Energy (2016) 1–15doi:10.1016/j.apenergy.2015.12.037.
URL http://linkinghub.elsevier.com/retrieve/pii/S0306261915016104

[37] S. Ikeda, R. Ooka, A New Optimization Strategy for the Operating Schedule of Energy Systems under Uncertainty of Renewable Energy Sources and Demand Changes, Energy and Buildings 125 (2016) 75–85. doi:10.1016/j.enbuild.2016.04.080.
URL http://linkinghub.elsevier.com/retrieve/pii/S0378778816303577

[38] C. D. Korkas, S. Baldi, I. Michailidis, E. B. Kosmatopoulos, Occupancy-based demand response and thermal comfort optimization in microgrids with renewable energy sources and energy storage, Applied Energy 163 (2016) 93–104. doi:10.1016/j.apenergy.2015.10.140.

[39] M. Ahmadi, J. M. Rosenberger, W.-J. Lee, A. Kulvanitchaiyanunt, Optimizing load control for a residential microgrid in a collaborative environment, IEEE Transactions on Smart Grid 6 (3) (2015) 1196–1207.

[40] A. Zidan, H. Gabbar, DG Mix and Energy Storage Units for Optimal Planning of Self-Sufficient Micro Energy Grids, Energies 9 (8) (2016) 616. doi:10.3390/en9080616.
URL http://www.mdpi.com/1996-1073/9/8/616

[41] R. De Coninck, R. Baetens, D. Saelens, a. Woyte, L. Helsen, Rule-based demand-side management of domestic hot water production with heat pumps in zero energy neighbourhoods, Journal of Building Performance Simulation 7 (4) (2014) 271–288. doi:10.1080/19401493.2013.801518.
URL http://www.tandfonline.com/doi/abs/10.1080/19401493.2013.801518

[42] H. Lund, W. Kempton, Integration of renewable energy into the transport and electricity sectors through V2G, Energy Policy 36 (9) (2008) 3578–3587. doi:10.1016/j.enpol.2008.06.007.

[43] P. J. Ramírez, D. Papadaskalopoulos, G. Strbac, Co-optimization of generation expansion planning and electric vehicles flexibility, IEEE Transactions on Smart Grid 7 (3) (2016) 1609–1619. doi:10.1109/TSG.2015.2506003.

[44] P. Denholm, M. Kuss, R. M. Margolis, Co-benefits of large scale plug-in hybrid electric vehicle and solar PV deployment, Journal of Power Sources 236 (2013) 350–356. doi:10.1016/j.jpowsour.2012.10.007.

[45] E. Sortomme, M. A. El-Sharkawi, Optimal scheduling of vehicle-to-grid energy and ancillary services, IEEE Transactions on Smart Grid 3 (1) (2012) 351–359. doi:10.1109/TSG.2011.2164099.

[46] E. L. Karfopoulos, K. A. Panourgias, N. D. Hatziargyriou, Distributed coordination of electric vehicles providing V2G services, IEEE Transactions on Power Systems 31 (1) (2016) 329–338. doi:10.1109/TPWRS.2015.2395723.

[47] M. Honarmand, A. Zakariazadeh, S. Jadid, Integrated scheduling of renewable generation and electric vehicles parking lot in a smart microgrid, Energy Conversion and Management 86 (2014) 745–755. doi:10.1016/j.enconman.2014.06.044.

[48] T. Wang, D. O'Neill, H. Kamath, Dynamic Control and Optimization of Distributed Energy Resources in a Microgrid, IEEE Transactions on Smart Grid (6) (2015) 2884–2894. doi:10.1109/TSG.2015.2430286.

[49] Y. Wang, B. Wang, C.-C. Chu, H. Pota, R. Gadh, Energy management for a commercial building microgrid with stationary and mobile battery storage, Energy and Buildings 116 (2016) 141–150. doi:10.1016/j.enbuild.2015.12.055.

[50] W. Su, J. Wang, J. Roh, Stochastic energy scheduling in microgrids with intermittent renewable energy resources, IEEE Transactions on Smart Grid 5 (4) (2014) 1876–1883. doi:10.1109/TSG.2013.2280645.

[51] P. Kou, D. Liang, L. Gao, F. Gao, Stochastic Coordination of Plug-In Electric Vehicles and Wind Turbines in Microgrid: A Model Predictive Control Approach, IEEE Transactions on Smart Grid 7 (3) (2016) 1537–1551. doi:10.1109/TSG.2015.2475316.

[52] O. Erdinc, N. G. Paterakis, T. D. P. Mendes, A. G. Bakirtzis, J. P. S. Catalão, Smart Household Operation Considering Bi-Directional EV and ESS Utilization, IEEE Transactions on Smart Grid 6 (3) (2015) 1281–1291. doi:10.1109/TSG.2014.2352650.

[53] L. Igualada, C. Corchero, M. Cruz-Zambrano, F. J. Heredia, Optimal energy management for a residential microgrid including a vehicle-to-grid system, IEEE Transactions on Smart Grid 5 (4) (2014) 2163–2172. doi:10.1109/TSG.2014.2318836.

[54] A. Dargahi, S. Ploix, A. Soroudi, F. Wurtz, Optimal household energy management using V2H flexibilities, COMPEL: The International Journal for Computation and Mathematics in Electrical and Electronic Engineering 33 (3) (2014) 7. doi:10.1108/COMPEL-10-2012-0223.

[55] A. Ouammi, Optimal power scheduling for a cooperative network of smart residential buildings, IEEE Transactions on Sustainable Energy PP (99) (2016) 1–1. doi:10.1109/TSTE.2016.2525728.

[56] M. Rastegar, M. Fotuhi-Firuzabad, H. Zareipour, M. Moeini-Aghtaie, A Probabilistic Energy Management Scheme for Renewable-Based Residential Energy Hubs, IEEE Transactions on Smart Griddoi:10.1109/TSG.2016.2518920.

[57] A. Rieger, R. Thummert, G. Fridgen, M. Kahlen, W. Ketter, Estimating the benefits of cooperation in a residential microgrid: A data-driven approach, Applied Energy 180 (2016) 130–141. doi:10.1016/j.apenergy.2016.07.105.
URL http://linkinghub.elsevier.com/retrieve/pii/S0306261916310431

[58] J. A. Peças Lopes, S. A. Polenz, C. L. Moreira, R. Cherkaoui, Identification of control and management strategies for LV unbalanced microgrids with plugged-in electric vehicles, Electric Power Systems Research 80 (8) (2010) 898–906. doi:10.1016/j.epsr.2009.12.013.

[59] S. B. Peterson, J. Whitacre, J. Apt, The economics of using plug-in hybrid electric vehicle battery packs for grid storage, Journal of Power Sources 195 (8) (2010) 2377–2384. doi:10.1016/j.jpowsour.2009.09.070.

[60] C. Zhou, K. Qian, M. Allan, W. Zhou, Modeling of the cost of EV battery wear due to V2G application in power systems, IEEE Transactions on Energy Conversion 26 (4) (2011) 1041–1050. doi:10.1109/TEC.2011.2159977.

[61] S. Han, S. Han, H. Aki, A practical battery wear model for electric vehicle charging applications, Applied Energy 113 (2014) 1100–1108. doi:10.1016/j.apenergy.2013.08.062.

[62] A. Kavousi-Fard, A. Khodaei, Efficient integration of plug-in electric vehicles via reconfigurable microgrids, Energy 111 (2016) 653–663. doi:10.1016/j.energy.2016.06.018.

[63] H. Farzin, M. Fotuhi-Firuzabad, M. Moeini, A Practical Scheme to Involve Degradation Cost of Lithium-ion Batteries in Vehicle-to-Grid Applications, IEEE Transactions on Sustainable Energydoi:10.1109/TSTE.2016.2558500.
URL http://ieeexplore.ieee.org/lpdocs/epic03/wrapper.htm?arnumber=7514958

[64] K. Smith, M. Earleywine, E. Wood, J. Neubauer, A. Pesaran, Comparison of plug-in hybrid electric vehicle battery life across geographies and drive cycles, Tech. Rep. 2012-01-0666, SAE (2012). doi:10.4271/2012-01-0666.
URL http://papers.sae.org/2012-01-0666/

[65] J. Neubauer, E. Wood, Thru-life impacts of driver aggression, climate, cabin thermal management, and battery thermal management on battery

electric vehicle utility, Journal of Power Sources 259 (2014) 262–275. doi:10.1016/j.jpowsour.2014.02.083.

[66] X. Liu, Z. Chen, C. Zhang, J. Wu, A novel temperature-compensated model for power Li-ion batteries with dual-particle-filter state of charge estimation, Applied Energy 123 (2014) 263–272. doi:10.1016/j.apenergy.2014.02.072.

[67] R. A. Lopes, J. Martins, D. Aelenei, C. P. Lima, A cooperative net zero energy community to improve load matching, Renewable Energy 93 (2016) 1–13. doi:10.1016/j.renene.2016.02.044.

[68] R. McKenna, E. Merkel, W. Fichtner, Energy autonomy in residential buildings: A techno-economic model-based analysis of the scale effects, Applied Energydoi:10.1016/j.apenergy.2016.03.062.

[69] C. Wouters, E. S. Fraga, A. M. James, An energy integrated, multi-microgrid, MILP (mixed-integer linear programming) approach for residential distributed energy system planning – A South Australian case-study, Energy 85 (2015) 30–44. doi:10.1016/j.energy.2015.03.051.

[70] X. Li, J. Wen, A. Malkawi, An operation optimization and decision framework for a building cluster with distributed energy systems, Applied Energy 178 (2016) 98–109. doi:10.1016/j.apenergy.2016.06.030.
URL http://linkinghub.elsevier.com/retrieve/pii/S0306261916308054

[71] L. Shen, Z. Li, Y. Sun, Performance evaluation of conventional demand response at building-group-level under different electricity pricings, Energy and Buildings 128 (2016) 143–154. doi:10.1016/j.enbuild.2016.06.082.
URL http://linkinghub.elsevier.com/retrieve/pii/S0378778816305710

[72] M. Ali, J. Jokisalo, K. Siren, A. Safdarian, M. Lehtonen, A User-centric Demand Response Framework for Residential Heating, Ventilation, and Air-conditioning Load Management, Electric Power Components and Systems 44 (1) (2016) 99–109. doi:10.1080/15325008.2015.1101726.

[73] Intelligence Energy Europe Project TABULA, National building typologies database, http://episcope.eu/building-typology/.

[74] S. Burke, Crawl spaces in wood framed single family dwellings in Sweden: unwanted yet popular, Structural Survey 25 (1) (2007) 51–60. doi:10.1108/02630800710740976.

[75] J. P. Zimmermann, End-use metering campaign in 400 households in sweden - assessment of the potential electricity savings, Tech. rep., Swedish Energy Agency (Sep 2009).

[76] L. Lundgren, K. Rydenstram, The swedish time use survey 1990/91, Tech. rep., Statistics Sweden (Oct 1992).

[77] American Society of Heating, Refrigerating and Air-Conditioning Engineers, Inc., 2009 ashrae handbook fundamentals inch-pound edition (2009).

[78] M. Molén, The swedish time use survey 2010/11, Tech. rep., Statistics Sweden (Jun 2012).

[79] P. D. Lund, H. Faninger-Lund, Integration of building and solar energy systems into one predesign tool, Presented at EUROSUN '98 (Sep 1998).

[80] Thomas Carlund, SMHI, Private communication (Nov 2014).

[81] B. W. Olesen, Radiant floor heating in theory and practice, ASHRAE Journal 44 (7) (2002) 19–26.

[82] L. Lu, X. Han, J. Li, J. Hua, M. Ouyang, A review on the key issues for lithium-ion battery management in electric vehicles, Journal of Power Sources 226 (2013) 272–288. doi:10.1016/j.jpowsour.2012.10.060.

[83] S. Santhanagopalan, K. Smith, J. Neubauer, G. Kim, A. Pesaran, M. Keyser, Design and Analysis of Large Lithium-Ion Battery Systems:, Artech House Publishers, 2014.

[84] L. Abramowski, A. Holmström, Res 2005-2006, the national travel survey, Tech. rep., Swedish Institute for Transport and Communications Analysis (Oct 2007).

[85] Idaho National Laboratory and U.S. Department of Energy, Advanced vehicle testing activity database, http://avt.inl.gov/.

[86] A. Cordoba-Arenas, S. Onori, Y. Guezennec, G. Rizzoni, Capacity and power fade cycle-life model for plug-in hybrid electric vehicle lithium-ion battery cells containing blended spinel and layered-oxide positive electrodes, Journal of Power Sources 278 (0) (2015) 473 – 483. doi:10.1016/j.jpowsour.2014.12.047.

[87] D. Andre, S.-J. Kim, P. Lamp, S. F. Lux, F. Maglia, O. Paschos, B. Stiaszny, Future generations of cathode materials: an automotive industry perspective, J. Mater. Chem. A 3 (13) (2015) 6709–6732. doi:10.1039/C5TA00361J.

[88] J. Dahn, G. M. Ehrlich, Lithium-ion batteries, in: T. B. Reddy (Ed.), Linden's Handbook of Batteries, McGraw-Hill, 2011, Ch. 26.

[89] I. Buchmann, Battery university. bu-205: Types of lithium-ion, http://batteryuniversity.com/learn/article/types_of_lithium_ion (Retrieved 26.5.2016).

[90] J. Wu, Y. Wang, X. Zhang, Z. Chen, A novel state of health estimation method of Li-ion battery using group method of data handling, Journal of Power Sources 327 (2016) 457–464. doi:10.1016/j.jpowsour.2016.07.065.

[91] J. Widén, Improved photovoltaic self-consumption with appliance scheduling in 200 single-family buildings, Applied Energy 126 (2014) 199–212. doi:10.1016/j.apenergy.2014.04.008.

[92] Nord Pool Spot, http://www.nordpoolspot.com/ (Retrieved 15.7.2014).

[93] European Energy Commission, Weekly oil bulletin newsletter, http://ec.europa.eu/energy/en/statistics/weekly-oil-bulletin (Retrieved 2.6.2015).

[94] U.S. Department of Energy, Alternative Fuels Data Center, Fuel properties comparison chart, http://www.afdc.energy.gov/fuels/fuel_comparison_chart.pdf (Retrieved 18.6.2015) (Oct 2014).

[95] U.S. Department of Energy, Where the energy goes: Hybrids, https://www.fueleconomy.gov/feg/atv-hev.shtml (Retrieved 22.7.2015).

[96] IBM Corp., IBM ILOG CPLEX Optimization Studio V12.4 documentation (2011).

[97] A. Myhr, T. Sehalic, Fordon 2014 (vehicles 2014), Tech. rep., Trafikanalys, http://trafa.se/PageDocuments/FORDON_2014.pdf (Retrieved 7.8.2015, in Swedish) (Mar 2014).

[98] I. Sartori, A. Napolitano, K. Voss, Net zero energy buildings: A consistent definition framework, Energy and Buildings 48 (2012) 220–232. doi:10.1016/j.enbuild.2012.01.032.

[99] B. Nykvist, M. Nilsson, Rapidly falling costs of battery packs for electric vehicles, Nature Climate Change 5 (April) (2015) 100–103. doi:10.1038/nclimate2564.

[100] T. Samad, E. Koch, P. Stluka, Automated Demand Response for Smart Buildings and Microgrids: The State of the Practice and Research Challenges, Proceedings of the IEEE 104 (4) (2016) 726–744. doi:10.1109/JPROC.2016.2520639.

[101] J. Käpylehto, Aurinkosähkön hyödyntäminen ja kannattavuus taloyhtiössä (use and profitability of solar electricity in housing cooperatives, in finnish), https://www.hsy.fi/fi/isannoitsijalle/neuvonta/Documents/Is.seminaari%202015/K%C3%A4pylehto_aurinkos%C3%A4hk%C3%B6.pdf (Retrieved 15.6.2016).

Supplementary Information
Flexibility of electric vehicles and space heating in net zero energy houses: an optimal control model with thermal dynamics and battery degradation

Jyri Salpakari[a,*], Topi Rasku[a], Juuso Lindgren[a], Peter D. Lund[a]

[a]*New Energy Technologies Group, Department of Applied Physics, School of Science, Aalto University, P.O.Box 15100, FI-00076 AALTO (Espoo), Finland*

This Supplementary Information contains details on the electricity consumption data, building and HVAC system models and parameters, and PEV models and parameters and driving time series generation.

S1. Electricity consumption data

The appliance and lighting electricity consumption data is from a monitoring campaign by the Swedish Energy Agency (SEA). The electricity consumption at 10-minute resolution of all the major electrical appliances in 201 detached houses and 188 apartments was measured on-site between August 2005 and December 2008 [1]. Most of the households were located in the Mälardalen region (58–59°N, 15–18°E). Even though the study was conducted several years ago, it is reasonable to assume that there have been no significant changes in residential electricity consumption since then, with the possible exception of lighting [2]. Data from ten detached houses measured for a full year was employed in this work. A significant part of the data was used at the simulation time corresponding to actual measurement, but the data had to be partially rearranged to obtain uninterrupted annual electricity consumption from September 2005 to August 2006 for each house. As the space heating and cooling loads of the houses are modeled separately, the resulting error is minor.

S2. Building and HVAC system models and parameters

The following dynamics for the nodes of the modeled houses h on time steps t are obtained by solving the energy balance equations of the two-capacity model.

*Corresponding author. Tel.: +358 50 433 1262, e-mail: jyri.salpakari@aalto.fi

The solution is written as equality constraints of an optimization problem.

$$\begin{aligned} T_{i,h,t+1} - \epsilon_{h,11} T_{i,h,t} - \epsilon_{h,12} T_{f,h,t} + \frac{\zeta_{h,11}}{C_{i,h}} (\alpha^+_{h,t} \psi^+_{h,t} - \alpha^-_h \psi^-_{h,t}) \\ = -\frac{\zeta_{h,11}}{C_{i,h}} (P_{app,h,t} + \varphi_{ppl,h,t} + \varphi_{sol,h,t} + H_{ie,h} T_{e,t}) \qquad \forall\, h, t, \\ - \frac{\zeta_{h,12}}{C_{f,h}} (H_{fe,h} T_{e,t}) \end{aligned} \tag{S1}$$

$$\begin{aligned} T_{f,h,t+1} - \epsilon_{h,21} T_{i,h,t} - \epsilon_{h,22} T_{f,h,t} + \frac{\zeta_{h,21}}{C_{i,h}} (\alpha^+_{h,t} \psi^+_{h,t} - \alpha^-_h \psi^-_{h,t}) \\ = -\frac{\zeta_{h,21}}{C_{i,h}} (P_{app,h,t} + \varphi_{ppl,h,t} + \varphi_{sol,h,t} + H_{ie,h} T_{e,t}) \qquad \forall\, h, t. \\ - \frac{\zeta_{h,22}}{C_{f,h}} (H_{fe,h} T_{e,t}) \end{aligned} \tag{S2}$$

The coefficients $\epsilon_{ij,h}$ and $\zeta_{ij,h}$ are elements of coefficient matrices $\boldsymbol{\epsilon}_h$ and $\boldsymbol{\zeta}_h$ on row i and column j:

$$\boldsymbol{\epsilon}_h = e^{\mathbf{B}_h \Delta t}, \tag{S3}$$

$$\boldsymbol{\zeta}_h = (\mathbf{I} - e^{\mathbf{B}_h \Delta t}) \mathbf{B}_h^{-1}, \tag{S4}$$

where

$$\mathbf{B}_h = \begin{bmatrix} -\frac{H_{ie,h} + H_{if,h}}{C_{i,h}} & \frac{H_{if,h}}{C_{i,h}} \\ \frac{H_{if,h}}{C_{f,h}} & -\frac{H_{fe,h} + H_{if,h}}{C_{f,h}} \end{bmatrix}. \tag{S5}$$

The above constraints are for radiator heating systems, and for the radiant floor heating systems the floor node is heated instead of the interior node: $\psi^+_{h,t}$ is multiplied by $\frac{\zeta_{h,12}}{C_{f,h}}$ instead of $\frac{\zeta_{h,11}}{C_{i,h}}$ in Eq.(S1), and by $\frac{\zeta_{h,22}}{C_{f,h}}$ instead of $\frac{\zeta_{h,21}}{C_{i,h}}$ in Eq. (S2). Cooling is provided to the interior node regardless of the heating system.

The parameters of the building envelopes are from a typical Swedish single-family building built in 1976–1985 in TABULA building typology [3]. The period 1976–1985 is the most representative of the 10 SEA houses in TABULA in terms of construction year. The building geometry [3] is scaled to the mean floor area of the 10 houses from SEA data, and the mean number of inhabitants in the SEA data is used (Table S1). The floor node heat capacities $C_{f,h}$ are calculated as the heat capacity of the concrete slab covering the total floor area $A_{fl,h}$ of the house, and the interior node heat capacities $C_{i,h}$ are calculated using the floor heat capacities as follows

$$C_{f,h} = c_c z_f A_{fl,h}, \tag{S6}$$

$$C_{i,h} = C_{ref} A_{fl,h} - C_{f,h}, \tag{S7}$$

where c_c is the volumetric heat capacity of concrete, and z_f is the thickness of the concrete floor slab. Slab thickness of $z_f = 8$ cm is found to be reasonable

considering the *TABULA* reference heat capacity C_{ref} [3], as well as typical underfloor heating system floor slab thickness of around 10 cm [4]. The heat transfer coefficients $H_{ij,h}$ between the temperature nodes i and j are calculated for each house h as follows [3, 5]

$$H_{if,h} = \bar{\upsilon} A_{fl,h}, \tag{S8}$$

$$H_{fe,h} = \left[\left(\frac{1}{U_{fl}} - \frac{1}{\bar{\upsilon}} \right)^{-1} + \Delta U_{tb} \right] A_{fl,h}, \tag{S9}$$

$$H_{ie,h} = c_a \mu h_{wa} A_{fl,h} + \sum_{p \in S_m} \Big[(U_p + \Delta U_{tb}) A_{p,h} \Big], \quad S_m = \{wi,\, do,\, ro,\, wa\}. \tag{S10}$$

$\bar{\upsilon}$ is the mean total heat transfer factor between the floor and the interior nodes, calculated with the model in [6] with mid-interval T_i and T_f, approximating operative temperature at 1.1 m height with T_i. U_p is the TABULA reference U-value of structural part p of house h, $A_{p,h}$ is the approximated surface area, ΔU_{tb} is the extra heat transfer due to thermal bridging, c_a is the volumetric specific heat capacity of air at 20°C, μ is the TABULA reference air exchange rate, and h_{wa} is the room height [7].

For a radiator system with sufficient oversizing, the supply and return temperatures at −15 °C external temperature can be lowered to 55/45 °C, instead of the typical 80/60 °C systems in Sweden [8]. For radiant floor heating systems the supply temperatures can be kept lower due to larger surface area of the floor

Table S1: Building dimensions used to model the detached houses.

$N_{ppl,h}$	A_{fl}	A_{wi}	A_{do}	A_{ro}	A_{wa}
3	145 m^2	25.5 m^2	2.3 m^2	145 m^2	116 m^2

Table S2: Building thermal parameters.

Symbol	Description	Value
c_c	Volumetric heat capacity of concrete	639 $\frac{\text{Wh}}{\text{Km}^3}$ [4]
c_a	Volumetric heat capacity of air at 20°C	0.34 $\frac{\text{Wh}}{\text{Km}^3}$ [5]
$\bar{\upsilon}$	Mean floor-interior heat transfer factor	8.56 $\frac{\text{W}}{\text{Km}^2}$
h_{wa}	Minimum residential dwelling room height	2.4 m [7]
C_{ref}	Reference heat capacity of a typical house	45 $\frac{\text{Wh}}{\text{Km}^2}$ [3]
μ	Reference air exchange rate	0.5 $\frac{1}{\text{h}}$ [3]
U_{wi}	Reference window U-value	0.76 $\frac{\text{W}}{\text{Km}^2}$ [3]
U_{do}	Reference door U-value	0.90 $\frac{\text{W}}{\text{Km}^2}$ [3]
U_{fl}	Reference floor U-value	0.20 $\frac{\text{W}}{\text{Km}^2}$ [3]
U_{ro}	Reference roof U-value	0.05 $\frac{\text{W}}{\text{Km}^2}$ [3]
U_{wa}	Reference walls U-value	0.15 $\frac{\text{W}}{\text{Km}^2}$ [3]
ΔU_{tb}	Extra heat transfer due to thermal bridging	0.10 $\frac{\text{W}}{\text{Km}^2}$ [3]

compared to that of the radiators, with typically 30–45 °C supply temperature at −26 °C external temperature [5]. In this work, the heating system supply temperature $T_{sup,t}$ is modeled as a piecewise linear function of the external temperature as

$$T_{sup,t} = \tau + \kappa T_{e,t}, \qquad T_{e,t} \leq 20°\text{C} \tag{S11}$$

$$T_{sup,t} = T_{sup,min}, \qquad T_{e,t} > 20°\text{C} \tag{S12}$$

where τ and κ are coefficients that depend on the type of hydronic heating system used.

The supply temperature curve for radiators is based on [8]. To determine the supply curve for floor heating, TRNSYS TYPE 653 simulations were conducted with heat exchanger efficiency $\epsilon = 0.6$ [9]. $T_{sup} - T_f = 10$ °C was found sufficient to transfer the thermal powers considered in this work (max. 10 kW) with plausible water flow values (max. 1.3 m/s) and pipe sizing (20 mm diameter, 20 cm spacing). The minimum supply temperature is set to $T_{sup,min} = 25$ °C for radiators and $T_{sup,min} = 39$ °C for floor heating in order to always allow the houses to be heated, enabling SHLC even in the summer. 45 °C supply temperature at −26 °C is used for floor heating.

The temperature dependent COP of the ground source heat pump $\alpha^+_{h,t}$ is modeled using the COP of a corresponding ideal Carnot heat pump cycle [10, 11]

$$\alpha^+_{h,t} = \eta_{Ca} \frac{T_g - \delta T}{T_{sup,t} + \delta T - (T_g - \delta T)} + 1. \tag{S13}$$

where $\eta_{Ca} = 0.55$ [11] is the Carnot efficiency and $\delta T = 5°\text{C}$ [10] is the temperature difference of the heat exchangers.

$T_g \approx 1°\text{C}$ is the annual average temperature of the borehole heat transfer fluid at the heat pump evaporator on the 25^{th} year of heat extraction, when the annual average has reached a steady state [12]. It has been obtained from Earth Energy Designer 2.0 [13] simulations of a typical 150 m deep borehole in normal Finnish bedrock, with 20 000 kWh annual heat requirement and no heat extraction in the summertime [12]. The 20 000 kWh annual heat demand closely matches the buildings studied in this work [3], and the 150-m borehole can provide sufficient thermal energy and power for our simulations [14]. The minimum monthly average fluid temperature during the year is approx. −3°C and the maximum 5–7 °C, depending on whether 1000 kWh of cooling is also provided by the borehole annually [12]. This amount of cooling does not affect the annual average T_g significantly [12]. Moreover, lower maximum monthly average fluid temperature would be expected for the case in this work, as heat is extracted in the summertime for DHW. As the heat capacity of the bedrock surrounding the borehole is massive compared to the heat capacity of the buildings, limited benefit is expected from adopting holistic modeling including the ground heat exchangers from models intended for designing GSHP systems [15].

Since the heat pump output temperature is assumed to be fixed to the supply water temperature of the heating system, the heating power is assumed to be

Table S3: HVAC system parameters.

Symbol	Description	Value
τ_{rad}	Radiator supply temperature parameter	549.4214 K
κ_{rad}	Radiator supply temperature parameter	-0.8571
τ_{rfh}	Floor heating supply temperature parameter	350.3768 K
κ_{rfh}	Floor heating supply temperature parameter	-0.1304
$\psi^{+}_{max,h}$	Heat pump maximum electric power	2.5 kW
η_{Ca}	Carnot efficiency parameter of the heat pump	0.55 [11]
δT	Heat exchanger temperature difference	5 K [10]
T_g	Yearly average borehole water temperature	1°C [12]
$\psi^{-}_{max,h}$	Cooling equipment maximum electric power	400 W
α^{-}_{h}	Ground source free cooling COP	30 [16]
$T_{max,i}$	Maximum interior node temperature	22°C [1]
$T_{min,i}$	Minimum interior node temperature	20°C [1]
$T_{max,f}$	Maximum floor node temperature	29°C [17]
$T_{min,f}$	Minimum floor node temperature	19°C [17]

controlled solely by adjusting the speed of the circulation pumps. Such controls might require special sizing of the floor heating system in practise.

The electricity consumption of heating DHW with the heat pump is calculated as

$$\psi_{dhw,h,t} = N_{ppl,h} \frac{\phi_{dhw,t}}{\alpha^{+}_{dhw}}, \qquad \forall\, h, t, \tag{S14}$$

where $N_{ppl,h}$ is the number of inhabitants in house h, $\phi_{dhw,t}$ is the thermal power required per person to heat the DHW and α^{+}_{dhw} is the COP of the heat pump when heating DHW, calculated with Eq. (S13). The heat pump operates in variable condensing between space heating and DHW inside the hourly time step [18].

In this work, the DHW storage tank is modelled as fully mixed at a constant temperature for simplicity, rendering α^{+}_{dhw} constant. The thermal power required for the DHW can thus be calculated as

$$\phi_{dhw,t} = V_{dhw,t}(c_{dhw}T_{dhw} - c_{in}T_{in}) + H_{dhw}(T_{dhw} - T_{max,i}), \tag{S15}$$

where $V_{dhw,t}$ is the volume of used DHW per person on hour t, c_{dhw} and c_{in} are the specific heat capacities and T_{dhw} and T_{in} are the temperatures of the hot water and cold inlet water respectively, H_{dhw} is the heat transfer coefficient between the DHW tank and its surroundings, and $T_{max,i}$ is the ambient temperature surrounding the tank, approximated here as the constant maximum permitted interior node temperature. H_{dhw} is calculated for a cylinder with radius-to-height ratio of 1:3, a volume of 180 l, and a U-value of 0.3 $\frac{\mathrm{W}}{\mathrm{Km}^2}$ [19]. The DHW tank losses are decoupled from the interior node for simplicity, corresponding to poor heat transfer from the e.g. storage area where the tank is located.

The DHW consumption time-series $V_{dhw,t}$ is constructed using hourly average DHW use profiles for workdays and weekends separately [20]. These profiles are based on measurements by the SEA in the Stockholm area between October 2006 and June 2007 [21], scaled to match the average daily DHW consumption of Swedish one-family houses of 42 l per person [22].

Table S4: DHW parameters.

Symbol	Description	Value
H_{dhw}	Heat transfer coefficient to ambient air	0.5387 $\frac{\mathrm{W}}{\mathrm{K}}$
T_{in}	Inlet water temperature	8°C [23]
T_{dhw}	Required hot water temperature	60°C [24]
c_{dhw}	Specific heat capacity of water at 60°C	1.14 $\frac{\mathrm{kWh}}{\mathrm{Km}^3}$ [5]
c_{in}	Specific heat capacity of water at 8°C	1.16 $\frac{\mathrm{kWh}}{\mathrm{Km}^3}$ [5]
α^{+}_{dhw}	Heat pump COP for DHW	3.15

S3. PEV models and parameters, and driving time series generation

The analytic solution of the PEV electricity balance equation is:

$$\begin{aligned}\frac{\nu}{1-e^{-\nu\Delta t}}(E_{v,t+1}-e^{-\nu\Delta t}E_{v,t})-\eta_b\eta_c(P^{+}_{v,t}+\eta_F F^{+}_{v,t}) \\ +P^{-}_{v,t}+\Psi^{\pm}_{v,t}=-D^{-}_{v,t}\end{aligned} \qquad \forall\, v,t, \tag{S16}$$

where v indexes the vehicles.

The following equality constraints are obtained by analytic solution of the two-capacity PEV thermal model:

$$\begin{aligned}&T_{b,v,t+1}-\beta_{11}T_{b,v,t}-\beta_{12}T_{c,v,t}+\frac{\gamma_{12}}{C_c}\Phi^{\pm}_{c,v,t} \\ &\quad+\frac{\gamma_{11}}{C_b}\left[\Phi^{\pm}_{b,v,t}+(1-\eta_b)(\Psi^{\pm}_{v,t}+\eta_c P^{+}_{v,t}+P^{-}_{v,t}+\eta_F\eta_c F^{+}_{v,t})\right] \qquad \forall\, v,t, \\ &\quad=-\frac{\gamma_{11}}{C_b}\left[H_{be}T_{e,t}+(1-\eta_b)D^{-}_{v,t}\right]-\frac{\gamma_{12}}{C_c}\left[H_{ce}T_{e,t}+\Lambda_c I_{sol,t}\right]\end{aligned} \tag{S17}$$

$$\begin{aligned}&T_{c,v,t+1}-\beta_{21}T_{b,v,t}-\beta_{22}T_{c,v,t}+\frac{\gamma_{22}}{C_c}\Phi^{\pm}_{c,v,t} \\ &\quad+\frac{\gamma_{21}}{C_b}\left[\Phi^{\pm}_{b,v,t}+(1-\eta_b)(\Psi^{\pm}_{v,t}+\eta_c P^{+}_{v,t}+P^{-}_{v,t}+\eta_F\eta_c F^{+}_{v,t})\right] \qquad \forall\, v,t, \\ &\quad=-\frac{\gamma_{21}}{C_b}\left[H_{be}T_{e,t}+(1-\eta_b)D^{-}_{v,t}\right]-\frac{\gamma_{22}}{C_c}\left[H_{ce}T_{e,t}+\Lambda_c I_{sol,t}\right]\end{aligned} \tag{S18}$$

where $T_{b,v,t}$ and $T_{c,v,t}$ are temperatures and C_b and C_c are the heat capacities of the battery ($_b$) and cabin ($_c$) nodes respectively, H_{be}, H_{bc}, and H_{ce} are the effective heat transfer coefficients between the nodes, $\Phi^{\pm}_{b,v,t}$ and $\Phi^{\pm}_{c,v,t}$ are the battery thermal management and cabin A/C total thermal power terms respectively, Λ_c is the effective surface area of the cabin, and finally $I_{sol,t}$ is the solar

irradiance. The coefficients β_{ij} and γ_{ij} are elements of coefficient matrices $\boldsymbol{\beta}$ and $\boldsymbol{\gamma}$ on row i and column j:

$$\boldsymbol{\beta} = e^{\mathbf{A}\Delta t}, \tag{S19}$$

$$\boldsymbol{\gamma} = (\mathbf{I} - e^{\mathbf{A}\Delta t})\mathbf{A}^{-1}, \tag{S20}$$

where

$$\mathbf{A} = \begin{bmatrix} -\frac{H_{be}+H_{bc}}{C_b} & \frac{H_{bc}}{C_b} \\ \frac{H_{bc}}{C_c} & -\frac{H_{ce}+H_{bc}}{C_c} \end{bmatrix}. \tag{S21}$$

The PEV driving patterns that determine the driving consumption $D^{-}_{v,t}$ are generated with probabilistic simulation based on data from a Swedish travel survey [25]. The travel survey was conducted between October 2005 and September 2006 on 41 000 randomly selected participants. Each participant recorded their movements on a single given day. The hourly distribution of journeys during the survey days (Figure S1) is employed here, as the raw travel journal data was not available for this work. Here, a journey is defined as a set of consecutive trips with either residence, workplace or school as final destination. The hourly journey data is categorized according to main purpose, as reported by participants.

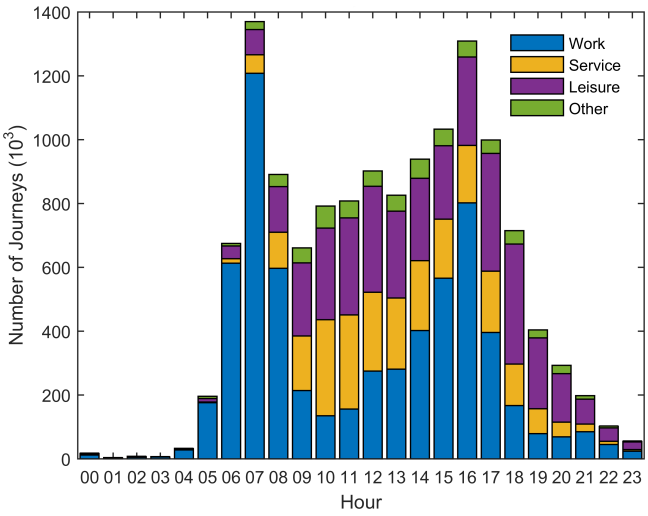

Figure S1: The hourly distribution of journeys by purpose [25].

The following assumptions are made to allow for extracting probability density functions (PDF) from the distribution, and determining the distances traveled:

1. The hourly distribution of passenger car journeys is the same as the hourly distribution of all journeys, except for a normalization factor.

2. Each PEV returns to home during the hour starting at 01.00 at the latest.
3. Each PEV goes to and returns from work once every weekday. Work journeys are not made on weekends. The hour starting at 11.00 is the latest hour to go to work, and the hour starting at 12.00 the first one to return from work.
4. Only one journey of each service (s), leisure (l), or other (o) type can be made during a single day.
5. After a service, leisure or other type of journey, the PEVs return to their location prior to the journey.
6. The lengths of the journeys are independent of the PEVs current location.
7. If multiple journeys are made on the same time step, only the longest journey will count.

Assumptions 1–3 allow for straightforward normalization of the work journey distribution to two PDFs for going to and returning from work. The PDFs of the other journey types are normalized with the numbers of corresponding types of journeys with passenger cars, and total traveling. The resulting PDFs are presented in Figure S2.

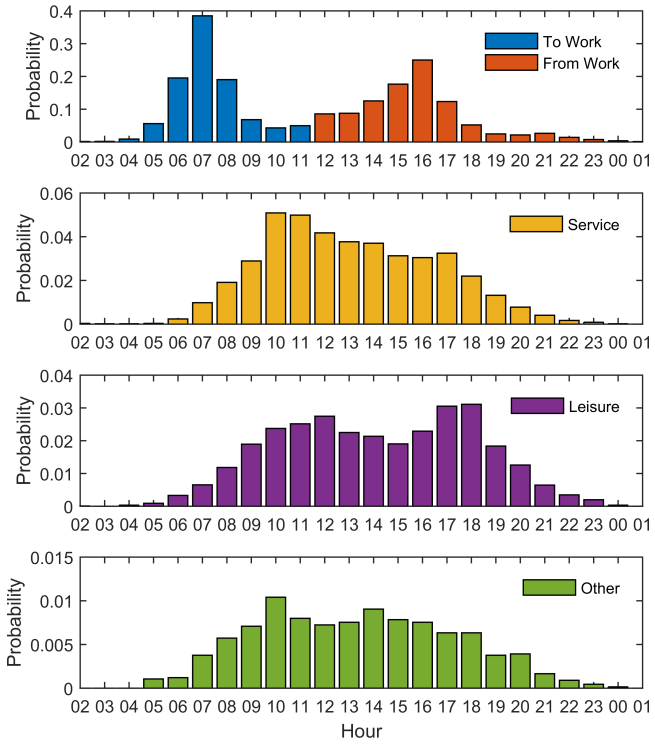

Figure S2: The journey PDFs. The PDF for work journeys is for weekdays; during weekends the probability is zero.

A PDF for work duration $f_w(\Delta t_w)$ (Figure S3) is obtained from the work journey PDFs for going to work $f_g(t_g)$ and returning from work $f_r(t_r)$:

$$f_w(\Delta t_w) = \sum_{t_g} f_g(t_g) f_r(t_g + \Delta t_w). \tag{S22}$$

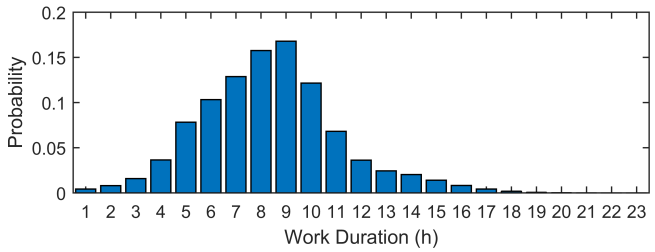

Figure S3: The PDF for work duration.

The PEV driving schedules are generated separately for each simulation day with inverse transform sampling of the cumulative distribution functions obtained from the PDFs, in accordance to the above assumptions. Average journey durations and lengths for journeys made by passenger car drivers [25] are employed. All the journeys take 1 h at hourly time resolution. To obtain time series for driving distance, the driving schedules are multiplied by the journey lengths, which are 24–51 km, depending on the purpose.

Tables S6 and S5 contain the technical parameter values used in PEV modeling.

Table S5: Vehicle-independent parameters used for the PEV modelling.

Symbol	Description	Value
ν	Hourly battery self-discharge rate	10^{-4} $\frac{1}{\mathrm{h}}$ [26]
$\psi^{+}_{max,b,v}$	Battery heating element max power	300 W [27]
$\psi^{-}_{max,b,v}$	Battery cooling element max power	1400 W [27]
$\psi^{+}_{max,c,v}$	Cabin heating element max power	4000 W [27]
$\psi^{-}_{max,c,v}$	Cabin cooling element max power	1800 W [27]
α^{+}_{b}	Battery heating element COP (PTC heater)	1 [27]
α^{-}_{b}	Battery cooling element COP (liquid cooled)	2.5 [27]
α^{+}_{c}	Cabin heating element COP (PTC heater)	1 [27]
α^{-}_{c}	Cabin cooling element COP (A/C)	2.5 [27]
C_c	Cabin heat capacity	28.3 $\frac{\mathrm{Wh}}{\mathrm{K}}$ [28]
H_{ce}	Heat transfer coefficient	22.6 $\frac{\mathrm{W}}{\mathrm{K}}$ [28]
Λ_c	Effective cabin surface area	0.77 m^2 [28]
$T_{max,c}$	Maximum driving cabin temperature	24°C [29]
$T_{min,c}$	Minimum driving cabin temperature	16°C [a]
$T_{max,b}$	Maximum battery temperature	45°C [26, 30]
$T_{min,b}$	Minimum battery temperature	15°C [b] [31, 30]
SOC_{min}	Minimum allowed battery SOC	0.25 [31]
SOC_{max}	Maximum allowed battery SOC	0.95 [31]

[a] Around 22°C in [29], excessive when passengers are appropriately clothed.

[b] Battery manufacturers allow temperatures down to −20 °C for discharging and 0 °C for charging for cells with LMO or NCM cathodes [26]. However, adverse low-temperature effects on battery performance are not significant above 15°C [30], and neither is degradation by Li plating, which the employed battery degradation model cannot describe [31].

Table S6: Vehicle-dependent parameters used for the PEVs modelled in this work.

Symbol	Description	2013 Chevrolet Volt (PHEV)	2013 Nissan Leaf (BEV)	High-End BEV [a]
$E_{max,v,0}$	Nominal battery capacity	16.5 kWh [32]	24.0 kWh [32]	70 kWh [33]
Q_{system}	Nominal battery Ah-capacity	45.0 Ah [32]	66.2 Ah [32]	193.1 Ah
U	Nominal battery voltage	355.2 V [32]	364.8 V [32]	366.0 V [33]
η_b	Battery efficiency[b]	$\sqrt{0.98}$ [32]	$\sqrt{0.98}$ [32]	$\sqrt{0.99}$ [32]
η_c	On-board charger efficiency	0.91 [32]	0.87 [32]	0.91 [32]
η_F	ICE energy conversion efficiency	0.3 [34]	0	0
$P^{\pm}_{max,v}$	On-board charger max. power	3.1 kW [29]	6.7 kW [29]	11.0 kW [35]
$F^{+}_{max,v}$	Fuel charging max. power	210 kW [32]	0 kW	0 kW
C_b	Battery heat capacity	43.57 $\frac{\text{Wh}}{\text{K}}$ [32, 36]	64.11 $\frac{\text{Wh}}{\text{K}}$ [32, 36]	185.9 $\frac{\text{Wh}}{\text{K}}$
H_{be}	Heat transfer coefficient	1.049 $\frac{\text{W}}{\text{K}}$ [28]	4.343 $\frac{\text{W}}{\text{K}}$ [28]	8.686 $\frac{\text{W}}{\text{K}}$
H_{bc}	Heat transfer coefficient	0.752 $\frac{\text{W}}{\text{K}}$ [28]	3.468 $\frac{\text{W}}{\text{K}}$ [28]	6.936 $\frac{\text{W}}{\text{K}}$
	UDDS driving consumption	157.6 $\frac{\text{Wh}}{\text{km}}$ [32]	125.1 $\frac{\text{Wh}}{\text{km}}$ [32]	170.4 $\frac{\text{Wh}}{\text{km}}$

[a] The High-End BEV is loosely based on the Tesla Model S, as full technical specifications of the Model S were not available, and parameters lacking a reference were scaled from Nissan Leaf parameters according to vehicle weight ratio [32], battery capacity ratio or battery area ratio [32, 33, 37].

[b] The square root of the battery efficiency is used, because the losses are applied equally when both charging and discharging the battery.

References

[1] J. P. Zimmermann, End-use metering campaign in 400 households in sweden - assessment of the potential electricity savings, Tech. rep., Swedish Energy Agency (Sep 2009).

[2] J. Widén, Improved photovoltaic self-consumption with appliance scheduling in 200 single-family buildings, Applied Energy 126 (2014) 199–212. doi:10.1016/j.apenergy.2014.04.008.

[3] Intelligence Energy Europe Project TABULA, National building typologies database, http://episcope.eu/building-typology/.

[4] J. Vinha, RIL 255-1-2014 Rakennusfysiikka 1, Rakennusfysikaalinen suunnittelu ja tutkimukset (Building physics 1, building physics design and research), Suomen Rakennusinsinöörien Liitto, RIL ry, 2014, (in Finnish).

[5] O. Seppänen, Rakennusten lämmitys (Heating of Buildings), Suomen LVI-yhdistysten liitto, 2001, (in Finnish).

[6] T. Cholewa, M. Rosiński, Z. Spik, M. R. Dudzińska, A. Siuta-Olcha, On the heat transfer coefficients between heated/cooled radiant floor and room, Energy and Buildingsdoi:10.1016/j.enbuild.2013.07.065.

[7] L. Holm, G. Essunger, SBN 1975 utgava 3, Svensk Byggnorm (Swedish Building Regulations 1975 3rd Edition), Statens Planverk, 1978, (in Swedish).

[8] P. L. J. Wollerstrand, P.-O. Johansson, Optimal reglering av radiatorsystem (optimal regulation of radiator systems), Tech. rep., Svensk Fjärrvärme AB, (in Swedish) (2007).

[9] T. Tuutti, Lämpödynaamisen mallin demonstrointi simuloidun lattialämmitysjärjestelmän ohjauksessa (demonstration of model based control in simulated floor heating system), master's thesis, Aalto University, (in Finnish) (2014).
URL http://urn.fi/URN:NBN:fi:aalto-201404161686

[10] H. F. Sullivan, Principles of vapour compression heat pumps, in: J. Berghmans (Ed.), Heat Pump Fundamentals, Martinus Nijhoff Publishers, The Hague, 1983, pp. 14–33.

[11] R. Wikstén, Lämpövoimaprosessit (Thermodynamic Processes), in Finnish, 4th Edition, Helsinki University Press, 2009.

[12] N. Leppäharju, Kalliolämmön hyödyntämiseen vaikuttavat geofysikaaliset ja geologiset tekijät (geophysical and geological factors affecting the use of bedrock heat), master's thesis, University of Oulu, (in Finnish) (Apr 2008).

[13] T. Blomberg, J. Claesson, P. Eskilson, G. Hellström, B. Sanner, Eed - earth energy designer, http://www.buildingphysics.com/index-filer/Page1099.htm (Retrieved 22.12.2016).

[14] NIBE Energy Systems, Ground source heat pump guide for one-family houses (in Finnish) (2014).
URL http://www.nibe.fi/upload/haato/Ohjeet/PIENTALOJENNIBEMLPOPAS1508-09.pdf

[15] W. Grassi, P. Conti, E. Schito, D. Testi, On sustainable and efficient design of ground-source heat pump systems, Journal of Physics: Conference Series 655 (012003). doi:10.1088/1742-6596/655/1/012003.

[16] K. Sirén, Jäähdytysjärjestelmien energialaskentaopas (energy calculation guide for cooling systems), Tech. rep., Finnish Ministry of the Environment, (in Finnish) (Sep 2011).

[17] B. W. Olesen, Radiant floor heating in theory and practice, ASHRAE Journal 44 (7) (2002) 19–26.

[18] J. Salpakari, P. Lund, Optimal and rule-based control strategies for energy flexibility in buildings with PV, Applied Energy 161 (2016) 425–436. doi:10.1016/j.apenergy.2015.10.036.

[19] S. Cao, A. Hasan, K. Sirén, Analysis and solution for renewable energy load matching for a single-family house, Energy and Buildings 65 (2013) 398–411. doi:10.1016/j.enbuild.2013.06.013.

[20] J. Widén, M. Lundh, I. Vassileva, E. Dahlquist, K. Ellegå rd, E. Wäckelgå rd, Constructing load profiles for household electricity and hot water from time-use data-Modelling approach and validation, Energy and Buildings 41 (7) (2009) 753–768. doi:10.1016/j.enbuild.2009.02.013.

[21] R. N. Å. Wahlström, U. Pettersson, Mätning av kall- och varmvatten i tio hushåll (measuring cold and hot water in ten households), Tech. rep., The Swedish Energy Agency, (in Swedish) (Apr 2008).

[22] T. Levander, L. Stengård, Mätning av kall- och varmvattenanvändning i 44 hushåll (measuring cold and hot water usage in 44 households), Tech. rep., The Swedish Energy Agency, (in Swedish) (Jul 2009).

[23] Norrköping Vatten och Avfall AB, Water quality reports, http://www.norrkopingvattenavfall.se/verksamhet/vatten/vattenkvalitet/ (Retrieved 24.6.2015).

[24] A. Larsson, Boverkets författningssamling, bfs2006:12, bbr12 (statute book by boverket), (in Swedish) (Apr 2006).

[25] L. Abramowski, A. Holmström, Res 2005-2006, the national travel survey, Tech. rep., Swedish Institute for Transport and Communications Analysis (Oct 2007).

[26] L. Lu, X. Han, J. Li, J. Hua, M. Ouyang, A review on the key issues for lithium-ion battery management in electric vehicles, Journal of Power Sources 226 (2013) 272–288. doi:10.1016/j.jpowsour.2012.10.060.

[27] J. Neubauer, E. Wood, Thru-life impacts of driver aggression, climate, cabin thermal management, and battery thermal management on battery electric vehicle utility, Journal of Power Sources 259 (2014) 262–275. doi:10.1016/j.jpowsour.2014.02.083.

[28] S. Santhanagopalan, K. Smith, J. Neubauer, G. Kim, A. Pesaran, M. Keyser, Design and Analysis of Large Lithium-Ion Battery Systems:, Artech House Publishers, 2014.

[29] Argonne National Laboratory and U.S. Department of Energy, Downloadable dynamometer database, http://www.anl.gov/energy-systems/group/downloadable-dynamometer-database.

[30] M. Dubarry, C. Truchot, B. Y. Liaw, K. Gering, S. Sazhin, D. Jamison, C. Michelbacher, Evaluation of Commercial Lithium-Ion Cells Based on Composite Positive Electrode for Plug-In Hybrid Electric Vehicle Applications: III. Effect of Thermal Excursions without Prolonged Thermal Aging, Journal of The Electrochemical Society 160 (1) (2013) A191–A199. doi:10.1149/2.063301jes.

[31] A. Cordoba-Arenas, S. Onori, Y. Guezennec, G. Rizzoni, Capacity and power fade cycle-life model for plug-in hybrid electric vehicle lithium-ion battery cells containing blended spinel and layered-oxide positive electrodes, Journal of Power Sources 278 (0) (2015) 473 – 483. doi:10.1016/j.jpowsour.2014.12.047.

[32] Idaho National Laboratory and U.S. Department of Energy, Advanced vehicle testing activity database, http://avt.inl.gov/.

[33] Tesla Motors, Inc., Tesla Model S Owner's Manual, http://www.teslamotors.com/sites/default/files/Model-S-Owners-Manual.pdf (Retrieved 12.8.2015) (2012).

[34] U.S. Department of Energy, Where the energy goes: Hybrids, https://www.fueleconomy.gov/feg/atv-hev.shtml (Retrieved 22.7.2015).

[35] Tesla Motors, Inc., Tesla Motors Sverige Website, Model S, http://www.teslamotors.com/sv_SE/models-charging#/basics (Retrieved 12.8.2015, in Swedish).

[36] A. A. Pesaran, Battery Thermal Management in EVs and HEVs : Issues and Solutions, Advanced Automotive Battery Conference (2001) 10.

[37] Nissan Motor Co., Ltd., 2013 Nissan LEAF Owner's Manual, https://owners.nissanusa.com/content/techpub/ManualsAndGuides/NissanLEAF/2013/2013-NissanLEAF-owner-manual.pdf (Retrieved 6.6.2016) (2012).